Analysis of Vortex Dynamics in Superfluid

by Rida Rambli

August 5, 2020

20 Credit Points
Supervisor : Dr Nugzar Suramlishvili

Abstract

The aim of this study is to observe the interaction between the quasiparticles and vortices in the superfluid ^{3}He-B system. Using the two-dimensional model, we measure the Andreev reflection of thermal quasiparticles in the ^{3}He-B incident upon the system of point vortices, where each vortex moves in the flow field generated by all other vortices.

Contents

1 Acknowledgement of Sources

For all ideas taken from other sources (books, articles, internet), the source of the ideas is mentioned in the main text and fully referenced at the end of the report. All material which is quoted essentially word-for-word from other sources is given in quotation marks and referenced. Pictures and diagrams copied from the internet or other sources are labelled with a reference to the web page,book, article etc.

Signed: Rida Rambli

Dated: 1st May 2018

2 Introduction

A pure superfluid in the zero-temperature limit has no viscosity. Atoms which have condensed into the ground state form the superfluid. In liquid ^{3}He and dilute Fermi gases, the condensate is formed by pairs of atoms known as Cooper pairs. Since in most superfluids, including ^{3}He-B, the superfluid velocity $\mathbf{v}$ is proportional to the gradient of the phase of wave function, $\nabla\theta$, and thus the superfluid is irrotational; $\nabla \times \mathbf{v} = \mathbf{0}$. However, superfluids can support line defects on which $\nabla \times \mathbf{v}$ is singular and these defects are known as quantum vortices. Around the vortex core, the phase θ of the wave function changes by 2π around the vortex core and hence gives rise to a circulating flow. A single quantum of circulation carried by each vortex is $\kappa = 2\pi\hbar/m$ where m denotes the mass of the constituent atoms or atom pairs (for superfluid ^{3}He-B,$\hbar$=1.054 $\times 10^{-}34$ J·s/rad and $\kappa = \pi h/m_3$= 0.662 $\times 10^{-7} m^2/s$ where m_3 represents the mass of a ^{3}He atom). [31]

At low temperatures, quantum vortices move with the local superfluid velocity [7]. Vortex tangle, which displays complex dynamics, is formed from the instabilities and reconnections of quantized vortices. This complex, disordered flow is known as quantum turbulence.

During the last two decades, there has been significant development in the experimental studies of quantum turbulence. The most ideal technique by far, which is being developed for superfluid ^{3}He-B utilizes the Andreev reflection of quasiparticle excitations from superfluid flow [15]. We present a combined numerical and experimental study of Andreev scattering from quantum turbulence in superfluid ^{3}He-B at ultralow temperatures and simulation of the evolution of moderately dense, two-dimensional, vortex tangles and the Andreev reflection of thermal quasiparticles excitations by these tangles [31]

In Chapter 3, we will introduce the fundamentals needed to understand the analysis of vortex dynamics in superfluid such as theoretical ideas and basic equations essential to solve the problems using methods of both classical and quantum mechanics. Moreover, there are further definitions and explanations of quantum dynamics which evolved from classical fluid dynamics in this section and also the formation and behavior of vortices in superfluid.

Chapter 4 explains the different phases that occur in both superfluid He-A and superfluid He-B. In this chapter, we will focus more on superfluid He-B where the BW state takes place. In Chapter 5, we describe the experimental techniques used to study Andreev reflection which has been conducted by University of Lancaster and Helsinki University of Technology by Ahonen, Haikala, Krusius and Lounasmaa [21]. While in Chapter 6, we study the Andreev reflection of the flux of thermal quasiparticles from the systems of point vortices in 2D and present the results and analysis of our numerical experiments we have run and recorded in MATLAB.

3 Fundamentals

3.1 Dynamics of superfluid

Quantum fluids are obtained at very low temperatures (close to absolute zero) where the properties liquids are formed due to the quantum effects. In this universe, there is only one element that remains in liquid form at absolute zero temperature, which is Helium [18]. There are two helium isotopes, ^{4}He and ^{3}He. We would only consider ^{3}He atoms, as they have a spin 1/2, due to the nucleus and obey Fermi-Dirac statistics.

As stated in the paper by A.J. Leggett,Quantum Liquids [20], there are two types of quantum liquids systems – Bose and Fermi quantum liquids. Bosons (liquid ^{4}He,the Bose alkali gases) undergo the phenomenon of Bose condensation and obey Bose-Einstein statistics while the fermion systems (liquid ^{3}He, electrons in metals) display the related phenomenon of Cooper pairing, which we will discuss further. Fermion system obey Fermi-Dirac statistics.

The elementary particles possess their own angular momentum-spin equal to $n\hbar/2$, n is integer including zero. For n even, the particles are bosons while for n odd, particles are fermions. As stated in a famous theorem of quantum field theory, the spin-statistics theorem [28], total wave function of any many-particle system must be even under the interchange of all the positions of any two boson of identical type and odd under interchange of any two identical fermions.

Stating this formally, if two particles of the same species labeled as i and j and their space and spin coordinates $\boldsymbol{r}_{\mathrm{i}}\sigma_{\mathrm{j}}$, we would obtain the following :

$$\Psi(r_1\sigma_1, r_2\sigma_2, ..., r_{\mathrm{i}}\sigma_{\mathrm{i}}, ..., r_{\mathrm{j}}\sigma_{\mathrm{j}}, ..., r_{\mathrm{N}}\sigma_{\mathrm{N}}) = \pm\Psi(r_2\sigma_2, r_1\sigma_1, ..., r_{\mathrm{i}}\sigma_{\mathrm{i}}, ..., r_{\mathrm{j}}\sigma_{\mathrm{j}}, ..., r_{\mathrm{N}}\sigma_{\mathrm{N}}) \tag{1}$$

Bosons are indicated by $+$ sign whilst fermions are indicated by $-$ sign. For free particles cases that can fill up plane wave states with momentum $\mathbf{k}$, spin projection σ and energy $\epsilon_{\mathrm{k}\sigma}$, the condition of equation stated above leads to a single-particles distribution $n_{\mathrm{k}\sigma}$ of the form

$$n_{k\sigma}(T, \mu) = [exp\beta(\epsilon_{k\sigma} - \mu) \mp 1]^{-1} \tag{2}$$

whereby μ is the chemical potential, $\beta = 1/k_BT$ (T is temperature and k_B is Boltzman constant) and here the $-$ sign indicates bosons, $+$ sign represents fermions. The equation with minus sign is stated as the Bose-Einstein distribution, whilst plus sign is indicated as the Fermi-Dirac distribution. Thus, this is the reason why boson are normally said to satisfy Bose statistics whilst fermions satisfy Fermi statistics. Before the phase transition to superfluid state, two fermions(or two ^{3}He atoms) have to create a boson called Cooper pair .

Superfluidity of ^{4}He was experimentally discovered by Kapitza, Allen and Misener in 1938. Although it is now believed that Kamerlingh Onnes must have had

superfluid Helium in his apparatus when he first liquefied Helium in Leiden in 1908. He and other pioneers of low-temperature physics soon discovered that below a critical temperature, T$\lambda \simeq 1K$, liquid helium displays unusual behavior. They therefore called it Helium I and Helium II, above and below this temperature respectively. [4]

L.D Landau(1941) developed the theory of superfluidity. The basis of the dynamics of Helium II is based on the fundamental result of the microscopic theory. At temperature except zero, Helium II behaves as if it possesses a mixture of two different liquids - superfluid and normal vicious fluid. It is important to note that no friction exists between these liquids in their relative motion, i.e. no momentum is transferred from one to the other.

It is fascinating to observe that unlike normal liquids, superfluid liquids at very low temperatures (below 2.17K or -270.98°C) have zero viscosity which flow without loss of kinetic energy. Atoms in this particular fluids will lose randomness unexpectedly and move in a coordinated manner in each movement. In result, this causes the fluids to lose all inner friction. This allows them to be stationary despite that their container is rotating, they flow through tiny pores in their container and also flow vertically upward like a fountain effect. This phenomena takes place because despite they have zero viscosity, they still have water tension, and hence leads to siphon effect.

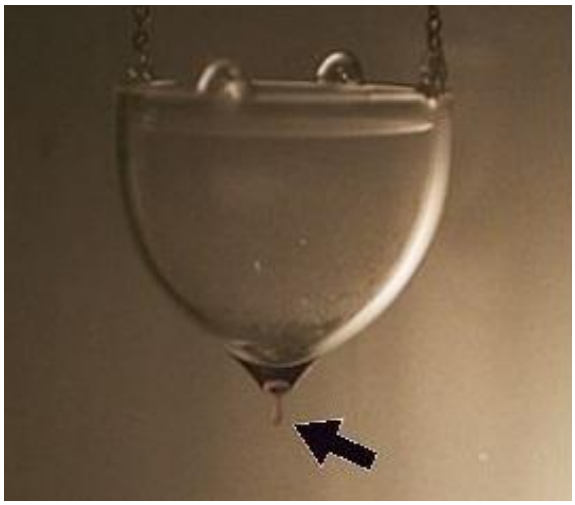

Figure 1: *Diagram shows the fountain effect possessed by a superfluid. Notice that liquid is escaping through the pores at the bottom of the container and the liquid moves upward. [1]*

3.2 Vorticity

Based on *Vortex Dynamics by P.G.Saffman*[24], in general the flow of a fluid is represented by a vector field $\mathbf{u}$(x,t) and the curl of the velocity is called the vorticity $\boldsymbol{\omega}$(x,t). In notations,

$$\boldsymbol{\omega}(\mathbf{x},t) = \omega_i \equiv \epsilon_{ijk}\frac{\partial u_k}{\partial x_j}$$
$$= \left(\frac{\partial w}{\partial y} - \frac{\partial v}{\partial z}, \frac{\partial u}{\partial z} - \frac{\partial w}{\partial x}, \frac{\partial v}{\partial x} - \frac{\partial u}{\partial y}\right) = (\xi, \eta, \zeta) \tag{3}$$

Based on the definiton that the velocity is solenoidal which is ;

$$\mathbf{div}\boldsymbol{\omega} = \frac{\partial \omega_i}{\partial x_i} = \frac{\partial \xi}{\partial x} + \frac{\partial \eta}{\partial y} + \frac{\partial \zeta}{\partial z} = 0 \tag{4}$$

The understanding and emphasis of vorticity for the definition of fluid motion comes from the following facts :

(i) inverting Eq.3 gives the velocity field as an integral over the vorticity field and (ii) neglecting the viscous diffusion of vorticity, the fluid is barotropic (meaning the density, ρ is a single-valued function of the pressure,P and the external forces are conservative), hence the vorticity satisfies the conservation principles commonly known as Helmholtz laws,(allowing the vorticity to be "followed").

Quantized vortex lines

This section is based on the book *Quantized Vortex Dynamics and Superfluid Turbulence* [11]. What makes the hydrodynamics of Helium II incredibly interesting is the quantization of the circulation of the superfluid. When Helium II rotates or moves faster than a critical velocity, superfluid vortex lines will emerge. This *vortex nucleation* procedure has been the interest of many investigations and can be found in the articles of Adams and Rica. Superfluid vortex lines can be either spatially organized (flow taking place along constant streamlines without turbulence) or disorganised(turbulent vortex tangles). The essential property of a superfluid vortex line which was disclosed by Onsager and later developed by Feynman, is that the circulation is quantised, in other words :

$$\int_{\mathcal{C}} \mathbf{v}_s \cdot \mathbf{dl} = \frac{h}{m} \tag{5}$$

where $\mathcal{C}$ is a circular path around the axis of the vortex. The *quantum of circulation* is denoted by the ratio $\Gamma = \frac{hbar}{m}$, h is Plank's constant and m denotes Helium mass. The straightforward way to create superfluid vortex lines is to spin a cylinder filled with Helium II at constant angular velocity Ω. Granted that Ω is large enough, superfluid vortex lines appear and form an ordered array of territorial density $n = 2\Omega/\Gamma$, hence along the axis of rotation all vortex lines are being aligned. In addition to this, the superfluid imitates the vorticity 2Ω of the solid body rotating normal fluid, with each vortex contributing one quantum to the total circulation.

3.3 First ideas about quantized circulation and vortices

In this section we will discuss both findings from both Onsager and Feynmann on circulation and vortices respectively which was carefully discussed by R.J Donelly in his book *Quantized Vortices in Helium II* [14].

Onsager's quantization of circulation

Lars Onsager introduced the idea of quantized circulation in superfluid Helium to students and colleagues at Yale University beginning around the year 1946. Onsager was conscious of the importance of scientific announcement and made public his discovery in a remark following a paper by Gorter on the two-fluid model. He said, in part, *' Thus the well-known invariant called the hydrodynamic circulation is quantized; the quantum of circulation is h/m...In the case of cylindrical symmetry, the angular momentum per particle is ħ'* (Onsager,1949)[14].

However, he did not follow his announcement with thorough papers. His next important remark on the subject came into sight in London's book on superfluid in 1954. An unpublished remark by Onsager at the 1948 Low Temperature Physics Conference quoted by London (London, 1954, p.151) and there Onsager considered the situation in the figure below .

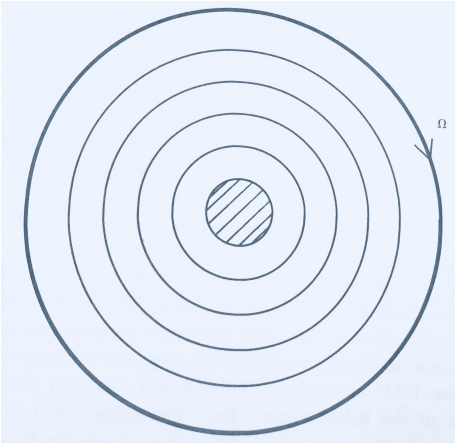

Figure 2: *Illustration above shows Onsager's early model for the rotation of a bucket of superfluid (London, 1954). The cross hatched at the central region is stationary and does not rotate. The area of the superflow in each successive ring of increasing radius have quanta of circulation k=1,2,3,....[14]*

A sequence of annular rings of radii $r_1, r_2, r_3, \ldots, r_n$ are drawn. We have mentioned that only for a simply-connected region, it contributes to the equations $\mathbf{v}$=0 and div ($\mathbf{v}$)=0 indicate the sole solution $\mathbf{v}$=0 under the boundary condition v=0. Consequently, for a cylindrical annular region we can use

$$v = grad \quad \varphi \tag{6}$$

and in quantum mechanics it requires that the increment of φ over a closed path has to be the integral multiple of $\hbar/m$. However, in the case of cylindrical symmetry, the potential is denoted by

$$\varphi = k\hbar\theta/m \tag{7}$$

whereby k is an integer and the azimuthal angle is denoted by θ. The velocity has a θ-component given by

$$v_k = \frac{1}{r}\frac{\partial \varphi}{\partial \theta} = \frac{k\hbar}{mr} \qquad (k = 0, \pm 1, \pm 2, \dots) \tag{8}$$

Now, picture a uniformly rotating bucket of radius R filled with liquid Helium at T=0 K. Imagine that the liquid can be divided up into series of concentratic cylindrical regions of radii $r_1, r_2, r_3, \dots, r_n$. In the region (r_k, r_{k-1}), we presume irrotational circulation, v_k, but allow discontinuities in the velocity at the interfaces. We must also consider that in the simply-connected central region ($r < r_1$) the velocity v_0 must disappear. Using a Lagrange multiplier method for N atoms in a Bose-Einstein degenerate state, it was used to calculate the minimum energy for such structure by London (1954). It has been achieved that for an angular velocity smaller than critical velocity

$$\Omega_c = \hbar/2mR^2, \tag{9}$$

the entire container will be contained with the stationary central region and this would require a period of rotation of

$$P > 8\pi^2 mR^2/\hbar = 8 \times 10^4 s \sim 1day \tag{10}$$

for a bucket of radius **R**=1cm. In addition to this, for angular velocities in excess of $\hbar/2mR^2$, we would have a series of cylindrical regions of different velocities which converge to Ωr for large values of k. Therefore, the system is rotating approximately as a whole with common angular velocity Ω as though it were a viscous liquid.

Feynman vortices

Richard Feynman (1955) was also working on the same problem and somewhat came to a different conclusion. He acknowledged that the vortices in the superfluid might take the appearance of a vortex filament with the core of atomic dimensions, which is truly a vortex line. The multiple connectivity of a vortex emerges because the superfluid is to some extent excluded from the core and circulates about the core in a quantized manner.

Feynman calculated the core radius assuming the core was hollow and determined it from surface tension of the fluid. Consequently, this has given him a core radius of $a \sim 0.5\mathring{A}$. He then estimates the energy per unit length of those vortices as

$$\epsilon = \int \frac{1}{2}\rho_s v_s^2 dr^2 = (\rho_s \kappa^2/4\pi) ln(b/a) \tag{11}$$

where ρ_s denotes the superfluid density, b is the radius of bucket or in the words the mean distance between vortices and v_s is the superfluid vorticity. This is a tremendous energy while the centrifugal force on each ring of fluid surrounding the core is balanced by a pressure gradient given by

$$dp/dr = \rho v^2/r = \rho \Gamma^2/4\pi^2 r^3 \tag{12}$$

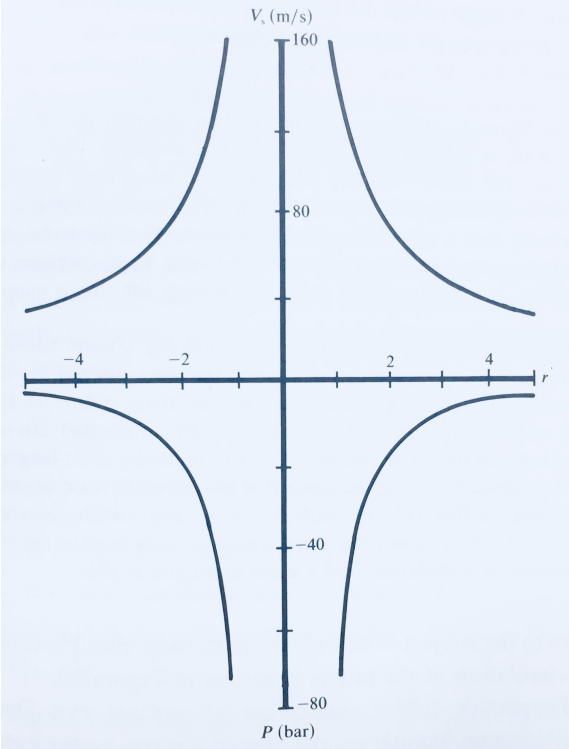

Figure 3: *Picture shows superfluid velocity and pressure distributions about a rectilinear vortex line located at r=0, having a core radius of 1 Å and circulation $\kappa = h/m$. In a real quantized vortex, the velocity usually does not exceed the Landau critical velocity of 60m/s((after Glaberson and Donnelly(1966)) [14]*

with $\Gamma = \kappa$. A sketch of the velocity and pressure distributions around a vortex line is illustated as in Figure 3.

Feynman (1955) also speculated how the vortex lines might be aligned. Initially, note that since the circulation κ enters squared in the energy in Eq.12, twice of quantized vortex line would have four times the energy of a singly quantized line and would likely be unstable to breakdown into four separate lines. Next, Feynman noted that in uniform rotation the curl of the velocity is the circulation per unit area, and the curl is 2Ω, hence there should be

$$n_0 = \frac{curl \quad v_s}{\kappa} = \frac{2\Omega}{\kappa} \sim 2 \times 10^3 \Omega lines/cm^2 \tag{13}$$

arranged parallel to the axis of rotation and with approximately uniform density. When Eq.13 is applied to more general flows, it is known as 'Feynman's rule'. Here, it mentions that the number of density of quantized vortex line is the ratio of the vorticity in the superfluid to the quantum of circulation. Feynman also considered the behavior of turbulence in the superfluid. His theories were brief and to the point :

In ordinary fluids flowing rapidly and with very low viscosity the phenomenon of turbulence sets in. A motion involving vorticity is unstable. The vortex lines twist about in an even more complex fashion, increasing their length at the expense of the kinetic energy of the main stream. That is, if a liquid is flowing at a uniform velocity and a vortex line is started somewhere upstream, this line is twisted into a

long complex tangle further downstream. To the uniform velocity is added a complex irregular velocity field. The energy for this is supplied by pressure head.

We may imagine that similar things happen in Helium. Except for distances of a few angstroms from the core of the vortex, the laws obeyed are those of classical hydrodynamics. A single line playing out from points in the wall upstream (both ends of the line terminate on the wall of course) can soon fill the tube with a tangle line.The energy needed to form the extra length of line is supplied by the pressure head.(The force that the pressure head exerts on the line acts eventually on the walls through the interaction on the lines with the walls). The resistance to flow somewhat above initial velocity must be the analogue in superfluid helium of turbulence, and a close analogue at that [14].

Despite the fact Feynman's(1955) conception of vortices uses Onsager's(1949) basic circulation hypothesis, the idea of discrete vortex lines leads to a widely different phenomenology.

3.4 Fermi quantum liquid

There are two types of quantum liquids as mentioned earlier, known as Bose and Fermi quantum liquid. Bose quantum liquid consists of atoms of integer spin whilst Fermi quantum liquid consists of atoms of half integer spin. An ideal Bose gas begins to condensate particles into the lowest available energy level in an environment below critical temperature.

Weak Van Der Waals forces bind Helium atoms into the liquid state at temperatures below 3.3K. However, below the Fermi temperature ($\simeq 1K$), the properties of normal liquid are qualitatively very similar to a weakly-interacting degenerate Fermi gas. Free Fermi gas (for a gas of free Fermions with mass m_e) the zero temperature ground state is obtained by filling all single particle states up to the Fermi energy.

Landau's basic idea was that [17] under deeply broad conditions, low-lying excitations of a system of interacting Fermions with repulsive interactions can be constructed starting from the low-lying states of a non-interacting Fermi liquid by a suitably slow "switching-on" of the interaction between the particles. The "switching-on" mechanism establishes a one-to-one analogy between the eigenstates of the system of ideal Fermi gas and a set of approximate eigenstates of the interacting system which is also often referred as "adiabatic switching-on".

Since the eigenstates of the on-interacting system are expressed by a set of occupation number $\left\{N_{\vec{k}\,\sigma}\right\}$ of single-particle momentum eigenstates, thus the corresponding low-lying excitations of the interacting system can be expressed by the same set of the occupation numbers. Since the adiabatic "switching-on" enables to introduce the concept of quasiparticles which is a particle surrounded by the cloud of interactions from all other particles. In this case, the strongly interacting system (quantum liquid) of particles is described as an ideal gas of quasiparticles with rescaled mass (effective mass of quasiparticle in liquid ^{3}He is m*≈3.1m where m is the bare mass of the atom).

The brilliance of Landau's founding was to recognise that, for the states that are weakly excited, which are close to the non-interacting Fermi distribution, the occupation number changes slowly even when particle-particle interactions are strong. The main repercussion of this fact is that the quantum numbers retain their validity as approximate quantum numbers, which actually indicate an excited state. Hence, low energy elementary excitations of an interacting Fermi liquid can be interpreted in terms of addition or removal of individual quasiparticles from a filled Fermi sphere of radius k_F.

For instance, outside the full Fermi sphere, a state of the ideal system consisting one quasiparticle of momentum $\hbar \overrightarrow{k}$ with $k \geq k_F$ evolves into an excited state of the interacting system containing one quasiparticle of momentum $\hbar \overrightarrow{k}$ outside the Fermi sphere. Furthermore, a state of the non-interacting system consisting of one empty state (a hole) of momentum $\hbar \overrightarrow{k}$ within the Fermi sphere evolves into an excited state of the interacting system which consists of a quasihole of the same momentum.

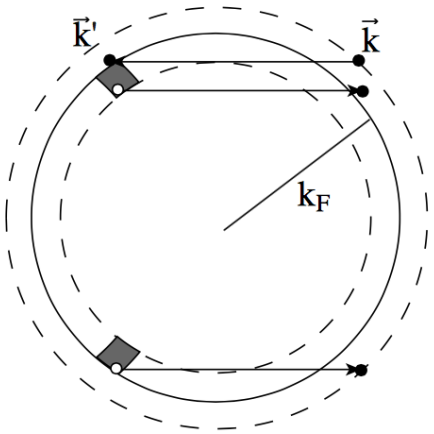

Figure 4: *Diagrammatic representation of Fermi sphere. Black dots correspond to quasiparticle excitation ($k > k_F$) and white dots correspond to quasiholes ($k < k_F$) [17]*

American physicists John Bardeen, Leon Cooper and John Robert Schrieffer (1957) proved that in superfluid state, electrons near the Fermi surface create pairs and construct a single quantum wave made of electron pairs with equal and opposite spins and momentums. These are known as Cooper pairs or in other words, pair condensates. Cooper pairs are easily separated by thermal energy and thus explains why the temperature must kept very low.

Superfluid quantum liquids vary from normal fluids in three aspects [10] :

(i) in quantum they possess a two-fluid behavior at non-zero temperature or in the presence of impurities,
(ii) they are inviscid which means they flow freely without the effect of viscous forces and
(iii) local rotation is restricted to discrete vortex lines of known strength, are continuous and can have arbitrary size, shape and strength).

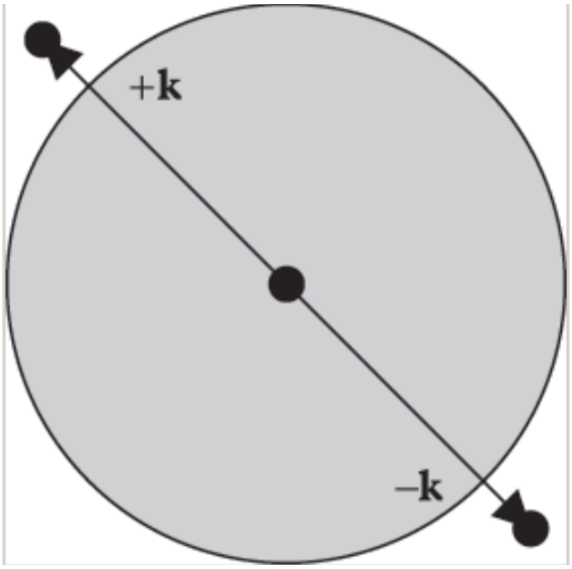

Figure 5: *Diagram demonstrates a pair of electrons with momenta +k and -k cooperating above a filled Fermi sea represented by the shaded region.[2]*

Quantum mechanics is the main reason for the difference in behavior for ^{3}He and ^{4}He. ^{4}He is a boson(integral spin and several bosons can occupy the same state) and thus the observation of ^{4}He superfluid phase is related to Bose condensation, whereby macroscopic fraction of atoms is in the lowest-energy state.

However, ^{3}He is a fermion (half integral spin electron) and according to the Pauli exclusion principle no more than one fermion can occupy the same one-particle state. Hence, the superfluidity exists due to the creation of weakly bound pairs of fermions(Cooper pairs) acting as bosons. We now examine Cooper's calculation. Let us represent the wave equation of the two electrons chosen, having the coordinates $\mathbf{r}_1$ and $\mathbf{r}_2$ respectively, in the form

$$\Psi(\mathbf{r}_1, \mathbf{r}_2) = \Phi_{\mathbf{q}}(\rho) e^{i\mathbf{q}\cdot\mathbf{R}} \chi(\sigma_1, \sigma_2) \tag{14}$$

where wave function in the center of the mass is denoted by $\Phi_{\mathbf{q}}(\rho)$, $\mathbf{R}$ is the center of mass coordinate and $\mathbf{R} \equiv (\mathbf{r}_1 + \mathbf{r}_2)/2$, $\mathbf{q}$ represents the wave vector of the center of the mass, $\rho \equiv \mathbf{r}_1 - \mathbf{r}_2$, σ_1 and σ_2 represent the spins of the two electrons either $\uparrow$ or $\downarrow$ and the spin wave function is denoted by χ (whereby any spin-orbit coupling is neglected) .

At the beginning, we restrict ourselves to the case $q = 0$ with respect to the Fermi sea and the center of the mass of the pair is at rest. From the fact that the singlet spin wave function is antisymmetric, then $\Phi_q(\rho)$ has to be symmetric in order to obey the Pauli principle whereby $\Phi_q(\rho) = \Phi_q(-\rho)$, and hence from this in turn requires that $\mathbf{g}(\mathbf{k}) = \mathbf{g}(-\mathbf{k})$. If there exists an orbital angular momentum correlated with the state, we could have numerous amplitudes, $\mathbf{g}_i(\mathbf{k})$, where the amplitudes of the multiple angular momentum associated with the state are denoted by `i`. Convincingly, it is possible that the electrons could pair in a triplet state, whereby $\chi_{\sigma_1\sigma_2} = \chi_{\sigma_2\sigma_1}$, and thus we would have amplitudes, $\mathbf{g}_i(\mathbf{k})$, which satisfy

$\mathsf{g}(\mathbf{k}) = \mathsf{g}(-\mathbf{k})$. In relation to this, the latter case occurs in ^{3}He.
Firstly, we will express Φ as a Fourier expansion,

$$\begin{aligned}\Phi(\rho) &= \sum_k \mathsf{g}(\mathbf{k})\mathsf{e}^{i\mathbf{k}\cdot\rho} \\ &= \sum_k \mathsf{g}(\mathbf{k})\mathsf{e}^{i\mathbf{k}\cdot\mathbf{r}_1}\mathsf{e}^{i\mathbf{k}\cdot\mathbf{r}_2} \end{aligned} \tag{15}$$

From Eq.15, it can be observed that the pair wave function can be regarded as consisting of plane wave states of equal and opposite momentum. In addition, for our assumed singlet pairing it is of opposite spins. For the pair wave function, the Schrödinger equation is

$$\Big[-\frac{\hbar^2}{2m}(\nabla_1^2+\nabla_2^2)+\mathtt{V}(\mathbf{r}_1,\mathbf{r}_2)\Big]\Psi(\mathbf{r}_1,\mathbf{r}_2) \tag{16}$$

$$= \Big(\epsilon + 2\frac{\hbar^2 k_F^2}{2m}\Big)\Psi(\mathbf{r}_1,\mathbf{r}_2) \tag{17}$$

where the energy, ϵ, is analogous to the combined energy of two electrons at the Fermi energy.

3.5 Turbulence

Turbulence is a flow regime in fluid dynamics described by chaotic changes in pressure in flow velocity. It can be felt for instance on an airplane or observed from fast flowing rivers. Turbulence is caused by excessive kinetic energy in parts of a fluid flow which overcome the damping effect of the fluid's viscosity. Therefore, turbulence appears to form easily in low viscosity fluids and more difficult in highly viscous fluids.[15]

The study of turbulence is abstract and requires a firm understanding of applied mathematics and physical grasp into the dynamics of fluids. We can observe the simplest and classic problem in this matter which concerns the disintegration energy in a cloud of turbulence. For example, when we stir a cup of tea and then leave it by itself, the turbulence in the cup could be observed to be decaying in time due to viscous dissipation.[13]

Laminar flow is the smooth and regular motion of a very viscous or slow-moving fluid. However, if the viscosity of fluid is not sufficiently high, or the characteristics speed is between moderate to large, then the motion of fluid will become irregular and chaotic and this is what we describe as turbulent. To characterise the turbulent we use Reynolds number $Re = UL/\mu$ where length scale is denoted by L, U is the velocity scale and kinematic viscosity is represented by μ.

3.6 Quantum Turbulence

Quantum turbulence and classical turbulence are similar in a way such that they are both in chaotic form of motion. However, their difference is that the quantum

Figure 6: *Turbulence in the tip vortex from an airplane wing . [22]*

turbulence is formed as chaotic tangle of quantised vortex filaments, where all vortices have the same strength.

Quantum turbulence occurs in quantum fluids. Unlike classical turbulence which is studied on the solid ground of Navier-Stokes equation, there is no particular equation to approach the motion for quantum turbulence. We could however, govern the motion through hierarchy of models at different length scales. Helium turbulence is characterized by wide separation of length scales $\xi \ll \ell \ll \mathcal{D}$, such that ξ is a measure of vortex core, ℓ is average distance between vortex lines and D is the size of system typically $\xi \approx 10^{-8}$m in He-B, $\ell \approx 10^{-5}$m and D $\approx 10^{-2}$m.

Quantum fluids are usually described as two interpenetrating fluids – a viscous normal fluid consisting of thermal quasiparticles similar to water and an inviscid superfluid exhibiting long-range quantum order. Every component has an apparent velocity field $\mathbf{v}_\mathrm{n}$,$\mathbf{v}_\mathrm{s}$ and temperature-dependent density ρ_n,ρ_s such that n stands for normal whilst s is superfluid. Regular viscous dissipation in the superfluid component does not take place; however the flow of a superfluid is akin to the resistance-free motion of electrons in a superconductor. This two-fluid model was first proposed for the explanation of phenomena related to He II which was introduces by Tisza[30] in 1938 and was then cultivated by Landau [19] in 1941 which included a hydrodynamic description.

Turbulence can exist in either of the fluid components. Behavior of the normal fluid can be observed to be identical from those described in classical fluids. However, turbulence in superfluid component is dominated by the quantum-mechanical constraints. In quantum mechanics, circulation around each vortex filament is described as κ=h/m, where h is Planck's constant, m is the mass of a fluid atom and κ is an integer multiple of the quantum circulation. Thus, turbulence in the superfluid component is dominated by a complicated, interacting tangle of quantized vortices of the same strength as shown below.[23]

As mentioned in *Kelvin-Wave Cascade on a Vortex in Superfluid* ^{4}He *at a Very Low Temperature*, for a quantum turbulent state, the significant length scales have a lower threshold provided the diameter of a quantized vortex core(10^-8 cm in He II,

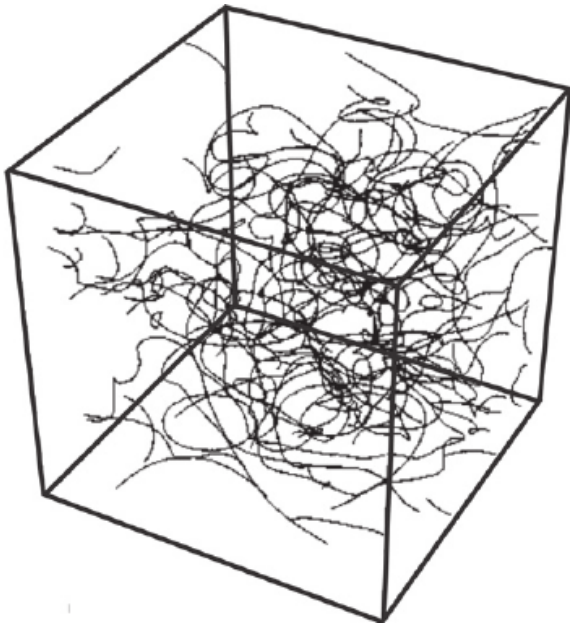

Figure 7: *Figure shows an evolving vortex tangle from the simulations of Tsubota et al.[33]*

except very near T_λ) and an upper bound of the system size(also known as typical intervortex spacing) of 1cm. The timescales produced are slowest by long-range vortex-vortex interactions (order of 1s) whereas the fastest are wave motions along quantized vortices with time less than $10^{-}9$s. These waves travel perpendicular to the direction of propagation or in general, transverse motion and circularly polarized displacements that are revived by vortex tension produced by kinetic energy per unit length of a quantized vortex. Kelvin waves along a straight line vortex posses an approximate dispersion relation given by [34]

$$\omega = \frac{\kappa k^2}{4\pi}[ln\frac{1}{ka_0} + c] \tag{18}$$

Vortex cutoff parameter is represented by a_0 and c is approximately 1. Seemingly, interaction of a wide breadth of spatial and temporal scales is involved in a quantized vortex tangle, thus as requisite for the system to be classified as turbulent.

4 Superfluid Phases of Liquid Helium

This chapter is extracted from *Turbulence Experiments in Superfluid ^{3}He at Very Low Temperatures* [15]. In a superfluid system, there exists two types of phases of liquid ^{3}He known as A phase and B phase. We will focus more on B phase later on. In A phase, the spin susceptibility is independent of temperature and is close to its value in the normal state. Meanwhile, B phase susceptibility tends to a finite value, which is nearly 1/3 of normal state value, as it approaches zero temperature.

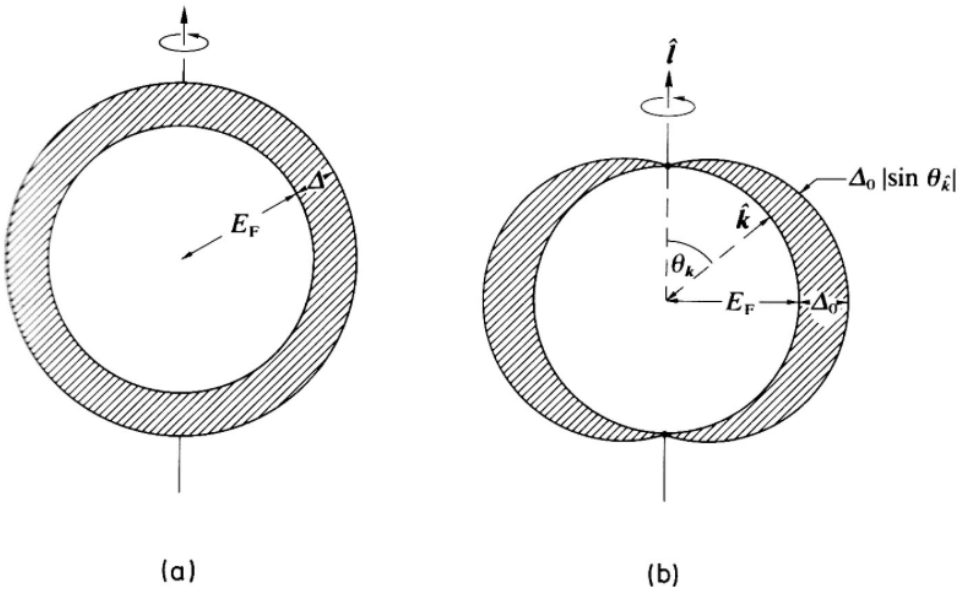

Figure 8: *Energy gap diagram of (a) the B phase and (b) the A phase. Observe that the gap vanishes along l direction in A phase [36]*

4.1 Superfluid He-A : The ABM State (A phase)

ABM state was first discussed by Anderson and Morel in 1961. This is the stable phase of a superfluid ^{3}He at higher pressures and temperature [15]. The magnetic susceptibility of ABM state is found to be very similar to normal state value. This phase is believed to consist of S_z=$\pm$1 pairs only, S_z denotes spin, S_z=0 does not appear in this phase, hence its free energy is reduced with respect to that of a B-phase by a strong magnetic field, which leads to 1st order phase transition (S_z=0 of B-phase are subdue completely) at pressure-dependent critical field of order 0.5T.

Order parameter of of ABM state is

$$\mathbf{d(k)} = \Delta_0 \hat{\mathbf{d}}(\hat{\mathbf{k}} \cdot \hat{\mathbf{m}} + i\hat{\mathbf{k}} \cdot \hat{\mathbf{n}}) \tag{19}$$

This state has a single preferred direction $\hat{\mathbf{d}}$ in spin space perpendicular to $\hat{\mathbf{S}}$. Unit vectors $\hat{\mathbf{m}}$ and $\hat{\mathbf{n}}$ are orthogonal and determine the directions in orbital space. The so-called orbital angular momentum vector, unit vector $\mathbf{l}$

$$\mathbf{l} = \hat{\mathbf{m}} \times \hat{\mathbf{n}}$$

The order parameter is complex and a rotation $\hat{\mathbf{m}}$ and $\hat{\mathbf{n}}$ about $\mathbf{l}$ describes a change of phase. Thus, in this phase a superfluid can be produced by orbital textures leading to a large variety of different vortex lines, including 'soft core' vortices which are doubly quantised with large cores defined by apparent textures[15]. The equation for the energy gap which is independent of the spin is

$$|\Delta(\mathbf{k})| = \Delta_0 |\hat{\mathbf{k}} \times \mathbf{l}| \tag{20}$$

Polar nodes exist in its energy gap in this phase along the **l** direction as shown in Figure 8 (b).

The spin up and spin down sub-systems of the A-phase act independently upon each other. The number density of up spin pairs at the expense of the down spin pairs is increased by the presence of a strong magnetic field, although the form of the energy gap does not depend on the spin states.

4.2 Superfluid He-B : The BW State (B phase)

Balian and Werthamer[3] in 1963 first discussed that the most uniform state in **k** space which is the spherically symmetric BW state. This state consists of equal number of pairs having three spin and orbital angular momentum projections, thus contributes to a total angular momentum **J**= **L** + **S**=0 with order parameter of

$$\mathbf{d(k)} = \mathrm{e}^{i\phi}\Delta\hat{\mathbf{k}} \tag{21}$$

It is very similar to a conventional superconductor as far as its thermal and mechanical properties are involved, but it's magnetic properties are far more complicated. Without the spin-orbit interactions, the original BW state is in fact degenerate with a set of states containing their spin and position axes rotate with respect to one another giving a vector order parameter

$$\mathbf{d(k)} = \mathrm{e}^{i\phi}\Delta\mathbf{R}(\mathbf{n},\theta)\hat{\mathbf{k}} \tag{22}$$

such that matrix $\mathbf{R}(\mathbf{n},\theta)$ defines a rotation about an axis **n** by an angle θ. Yet, the Cooper pairs are in a state of indefinite total angular momentum, thus there exist now a superposition of J=0,1,2 states, J denotes the angular momentum. The angular variable ϕ in the exponential term denotes the phase of the order parameter and the gradient of this determines the superfluid velocity ($\mathbf{v}_s \sim \nabla\phi$). B phase in low magnetic fields is explained greatly by BW state with a rotation angle, which is also called as Leggett angle,θ, such that

$$\theta = \arccos(-1/4) = 140^\circ \tag{23}$$

is calculated by minimising the dipolar free energy.

Experimentally, the B-phase is indeed the stable state in low fields except at high pressures and temperatures. Hence, we indicate here that the flow properties of the low field B-phase are very uncomplicated. They are defined by the phase of the order parameter directly corresponding to ^{4}He. The vortex lines in the B-phase are also particularly simple which are formed by a change of 2π of the phase of the order parameter around central core region with a size of order of coherence length.

When a magnetic field is applied to a normal degenerate Fermi gas, the Fermi momenta for the up and down spin particles are split. This allows the Fermi gas energies to equalise after the added magnetisation energy as there will be more spin up particles than spin down particles. In the B-phase, in the spin-triplet (S=1) states,

the Cooper pairs are formed. One third of these have S_z=0 where the z-axis is along the direction of the net magnetisation. These pairs form a symmetric superposition of spin up and spin down quasiparticles and hence require the Fermi momenta of the two spin sub-systems to be identical.

Since these pairs lead to a magnetisation reduction in a similar manner as the pairs of spin singlet superfluid, one might assume that at T=0 the static magnetisation is reduced to 2/3 of its normal state value. However, this is true only in the absence of Fermi liquid corrections. In practice, susceptibility is reduced to approximately 1/3 of its normal state value at T=0.

Elimination of the energy gap is produced by suppression of the S_z=0. This leads to an anisotropy (directionally dependent) of an energy gap and abide to superfluid properties. The anisotropy is big in high magnetic fields (otherwise it is usually small). The thermal and magnetic properties are weakly affected. An induced orbital angular momentum exists along the anisotropy axis $\hat{\ell}$. The direction $\hat{\ell}$ and **n** are dependent often by external boundary conditions such as magnetic field, cell walls and normal-superfluid counterflow. Thus these vectors generally vary throughout the experimental cell leading to magnetic and orbital textures.

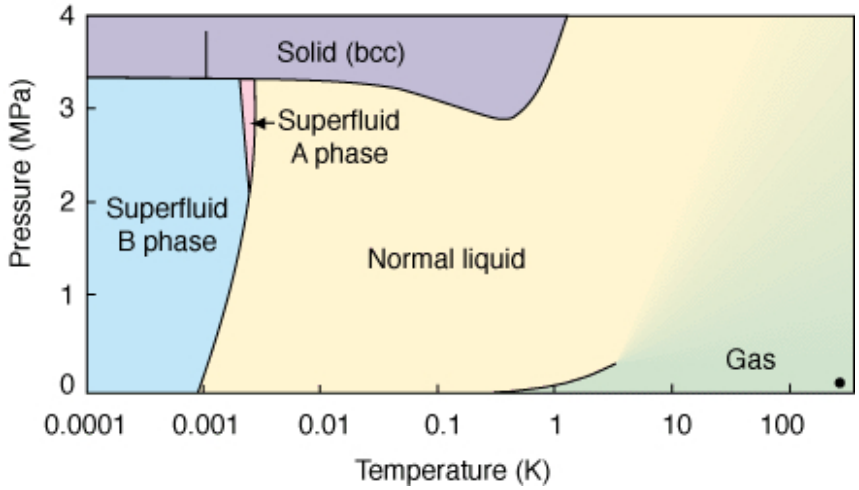

Figure 9: *.Diagram shows phases in ^{3}He. At the end of the lower right corner indicates room temperature and pressure. As we have discussed, there are phases of ^{3}He, A and B. [29]*

5 Experimental Techniques

This chapter is extracted from the book *Progress in Low Temperature Physics* by Richard Phillips Feynman[23]. The experimental technique, and its theoretical bases, discussed in this section are the only form of experiment to study quantized vortices and quantum turbulence in a superfluid in very low temperature.

5.1 Andreev scattering of a quasiparticle beam

For studies of quantum turbulence, as stated in [16], it is ideal to choose superfluid He-B since its mechanical properties are quite simple and its vortices are quite easy to observe even at very low temperatures. Since Andreev scattering (Andreev,1964; Enrico et al.,1993) of quasiparticles by the flow field is so strong, we can easily detect vortices by the reflected quasiparticles. This system provides us a very powerful tool for studying vortices and turbulence in very low temperature regime.

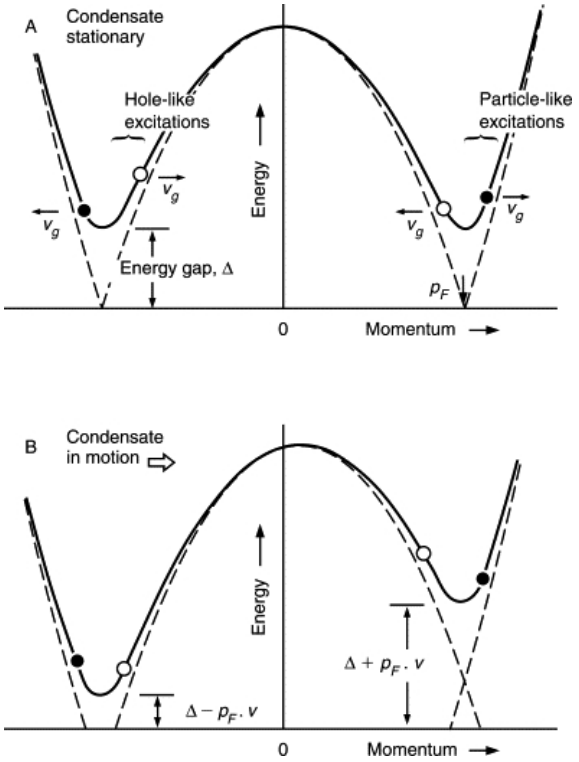

Figure 10: *Figure shows the excitations dispersion curve of quasiparticles. (A)two classes of excitations exist for stationary condensate : group velocity of quasiparticles parallel to momentum (black circles) and group velocity of quasiholes antiparallel to momentum. (B) condensate moves relative to observer, Galilean transformation tip the dispersion curve [16]*

As shown in Figure 10, let us consider the dispersion curve of the ^{3}He quasiparticle excitations. Here the dispersion curve is tied to the reference frame of the superfluid condensate, which leads to a frame moving with respect to the condensate. The curve becomes tilted, since in this moving frame (as shown in Figure 10(B)) the excitation energies undergo a Galilean transformation :

$$E(\mathbf{p}) \rightarrow E(\mathbf{p}) + \mathbf{p} \cdot \mathbf{v} \tag{24}$$

The idea behind Figure 10 is that in the absence of the flow, the energy gap is symmetrical for quasiparticles and quasiholes regardless of their motion. When the super flow is present (super flow velocity is $\mathbf{v}$) then the energy gap $(\Delta + \mathbf{p} \cdot \mathbf{v})$ effectively increases for particles moving in the direction of the flow and decreases for the particles moving in opposite direction.

The effective potential experienced by the quasiparticle excitations or in other words the appropriate minimum in the dispersion curve varies with the local liquid velocity as

$$E_{\min} = \Delta + \mathbf{p} \cdot \mathbf{v}(\mathbf{r}) \tag{25}$$

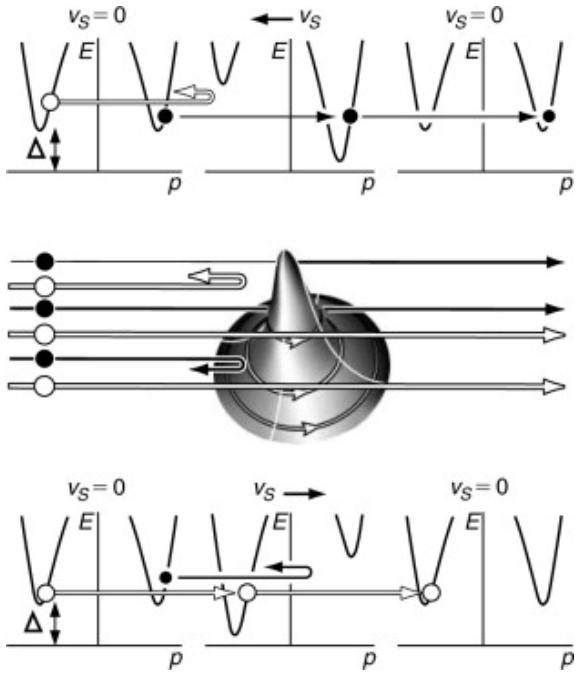

Figure 11: *Center figure: Quasiholes pass below the vortex while a fraction of quasiparticles are reflected forming an excitation shadow, whilst above the vortex, quasiparticles pass unrestricted but a fraction of quasiholes are Andreev reflected.Top figure: Incident occurring on the upper part of vortex shown in Center figure. Bottom figure : Incident occurring on the lower part of vortex shown in Center figure. [23]*

A local barrier to excitations is thus presented by the flow field around a vortex with the appropriate momentum direction. If the barrier height is higher than energy of an incoming excitation, the Andreev reflection takes place. Thus this effect allows us to detect vortices.

The study of vortex presence is shown in Figure 11 . As a first step, we would consider an incident of excitations on the upper side of the vortex from the left. For the stationary fluid, appropriate dispersion curves (left and right) and for moving superfluid close to the vortex the dispersion curve is figure center. Because the tipping of dispersion curve is downwards for quasiparticles moving to the right, their excitations pass through the flow freely. Thus, on the top side of the vortex line, there is full flux transmission of quasiparticles.

However, for the quasihole on the top left, there are higher energies for the dispersion curve which leads to the presentation of an effective energy barrier. Consequently, the quasihole does not consume sufficient energy to pass if it goes through too close to the core, i.e where there is higher flow of velocity. The energy of the quasihole in the superfluid reference frame decline towards the energy minimum which is also known as the energy gap, Δ and its group velocity decreases as the quasihole approaches the core. If the quasihole has insufficient energy (has zero group velocity), energy in the condensate frame equals to the energy gap at some point.

Around the bottom of the dispersion curve, there is an effective push of the excitation by the flow gradient, thus it develops as a quasiparticle, in the opposite direction with a group velocity. The excitation trajectory is in the opposite direction whilst the momentum transfer is remarkably small to the point that it is ignored. Hence, this relatively ideal retro-reflection is known as Andreev reflection or Andreev scattering.

5.2 Vibrating Wire Techniques

Vibrating wire techniques have been developed in Lancaster, specifically to probe the very dilute excitation gas in superfluid ^{3}He at the lowest achievable temperatures, for many years.[16]

Vibrating wire Resonator Design and Construction :
There are several **reasons** why at low temperatures in Helium liquids, vibrating wire resonators work well.

(i) Even over large range of sensitivity, they measure directly the response of the fluid to mechanical motion.
(ii) No significant heat leaks occur into the experimental volume, thus allowing very low temperatures to be achieved.
(iii) They are able to resolve temperature changes of order 1nK.
(iv) Power dissipations in the B-phase with a resolution of order 10 fW can be measured, including vortex lines and turbulence.

Very fine superconducting wires with high Q factors (quality factors is the parameter that indicates the power dissipation in accelerating cavities) have been used to study temperatures down to $T_C/9$ in pure ^{3}He, where the damping on the wire resonator is less than that which can be achieved in a vacuum at 1K.

Types of wires:
Generally, there are two types of wires used to make resonators which are pure tantalum and niobium-titanium. They are chosen because of their superconducting ability under the experimental conditions used so far (i.e magnetic fields no greater than 0.6T). The niobium-titanium resonators comprise a single filament separated from copper-clad filamentary wire with dimensions ranging from 4.5μm to 13μm whilst tantalum wire is bare with diameter of 125μm.

Techniques used in vibrating wires:

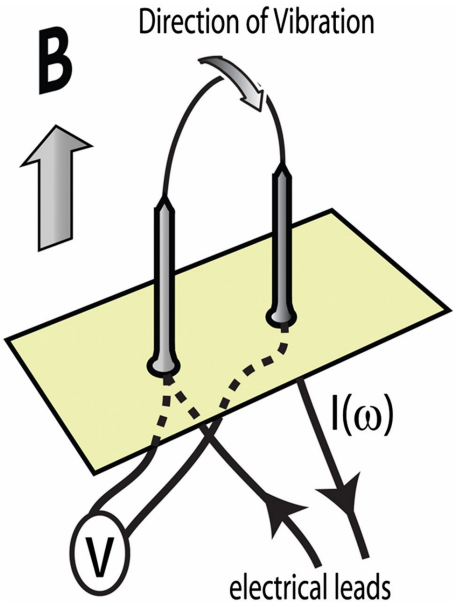

Figure 12: *Figure shows a schematic diagram of a vibrating wire resonator.[35]*

As shown in Figure 12, it is a NbTi (niobium-titanium) vibrating wire set up. For the construction; first, inner cells are made by creating two pin-holes in a piece of stycast-impregnated paper. A loop on one side is formed by stripping off the copper-clad NbTi filamentary wire from its insulating material and threading through the holes. A cylindrical metal bar with an equal diameter to the leg spacing is passed through the loop and paper base. A well-defined shape of a semicircle with a diameter (referred as leg spacing), on 'legs' with a length equal to half the leg spacing, is created by tightening the loop around the bar. Stycast plays an important role to hold the wire firm and to form a superleak-tight seal by running it into the pin-holes.

The bar is then taken away and copper-clad is stripped off the top of the loop by nitric acid leaving stiff copper-clad legs, with a length of about one third the leg spacing at the base of the loop. Now, there would be 60 or so free filaments of diameter 4.5μm to 13μm looped across the legs. They are picked off, one by one, with the help of a microscope with fine tweezers. Finally, it is expected that a single

filament remains to form the vibrating wire. At the broken end of the discarded filaments, two blobs of stycast are put over them, forming a seal and to stop any broken filament ends from interfering with the movement of the active filament. The resonator is now ready for gluing into the inner cell. For the construction of a Ta (tantalum) vibrating wire, it follows the same lines, however it is less complicated since there are no filaments.

5.3 Detection of a Cloud of Vorticity around a Vibrating Wire Resonator

In this section, we will discuss about detecting a vortex tangle by a vibrating wire resonator. In the vibrating wire resonator set up, Faraday voltage is generated through the movement of wires through the field and it is proportional to its velocity. It is measured using a lock-in amplifier. Damping is the quantity usually needed to be measured with a vibrating wire which determines the frequency width Δf_2 of the resonance line.

The effect of vortices is detected on the vibrating wire damping. At low temperature in B-phase, thermal damping appear from the normal scattering of ballistic excitations at the wire surface. However, orders of magnitude by Andreev reflection of excitations enhance the thermal damping by the superfluid back flow around the wire.

It is important to know that on the wire, the damping is a sensitive measure of the flux of excitations incident. As this flux changes promptly with temperature, dominated by the Bolzmann factor, the wires are treated as very sensitive thermometers at very low temperatures .

In this section, discussion will be made upon the Figure 13. It is a simplified one-dimensional scenario representing interactions if quasiparticles with a vibrating wire resonator in the presence of vortex lines.

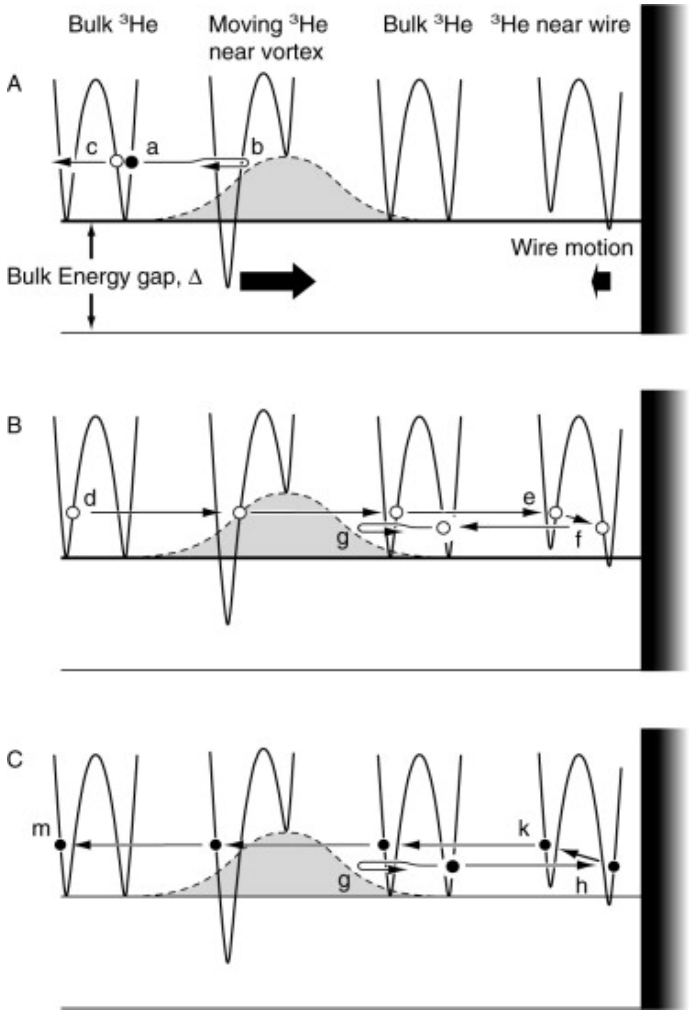

Figure 13: *Trajectories of excitations approaching a moving wire in the vicinity of a flow field which tips the dispersion curve locally [16].*

In top section, A:

The right side of the diagram shows a vibrating wire surface moving slowly to the left taking the liquid near the surface together with it, causing a slightly tilted dispersion curve near the wire. Around the wire we have another region of right-ward flow which is generated by a nearby vortex giving a tilted dispersion curve, and in between we have a bulk undisturbed liquid with no dispersion curve tilt. It can be observed from the figure that the right-hand side of the dispersion curve rises, and this barrier acts on rightward-traveling quasiparticles and leftward-traveling quasiparticles. Here, all incoming excitations are incident from the left.

Two classes of incoming excitations:
(i) Quasiparticles with momenta in the rightward direction.
(ii) Quasiholes with momenta in the reverse direction.

For the first case in A, an incoming quasiparticles at position 'a' enters the flow field from the vortex and encounter an increasing barrier which it cannot surpass. At 'b', it is Andreev reflected and backtrack its path, and it is then now a quasihole,'c'. Therefore all low-energy incoming quasiparticles are Andreev reflected and

will never arrive at the wire surface to exchange momentum with the wire. Condensate has a very limited capacity for absorbing the excitation momentum and the incoming quasiparticle and the outgoing quasihole have virtually equal momenta, except the group velocity is reversed.

Middle section, B:
At 'd' there is an incident quasihole which being on the other side of the dispersion curve, does not experience any potential barrier. It travels all the way to the wire surface where it normally scattered to 'e' and 'f', exchanging -$2p_F$ of momentum with the wire. For a quasihole, it exchanges negative momentum, and pulls the wire instead of pushing. Because the scattering process is elastic within the wire frame, this reflects upon the small jump in energy on scattering at the wire surface. The quasihole backtrack its path, but now it acknowledges the potential barrier and is Andreev reflected back to the wire at 'g'. Its consecutive trajectory continues in the lower section C.

Lower section, C:
At 'g', it goes back to the wire as a quasiparticle, is now scattered to from 'h' to 'k', exchanging $2p_F$ of momentum with the wire. It ignores the potential barrier and emerges at 'm' still as a quasiparticle. The net result of this observation is that the excitation arises with virtually the same initial momentum, and the two normal scattering processes at the wire surface cancel out. Again, there is no exchange of momentum with the wire for all low-energy incident quasiholes.

It is shown that if the flow field were of opposite directions, the same reasons would hold with the particle flavours exchanged which also includes the particles incident on the wire from the rear rather than the front. No matter the configuration of flow regions, both flavours of low-energy excitations will rise with virtually the same momentum as they had on entry and so will not damp the wire movement.

Summing over all three sections of the figure, there are two incoming and two outgoing excitations in both of the two regions of the two sides of the barrier. The particle-hole symmetry is fixed as the net momentum of all trajectories in the two regions is zero. How momentum is exchanged between the wire and thermal quasiparticle excitations is influenced by the flow field of surrounding vortices. However, if the momentum exchange by low-energy excitations is removed, it results in a proportionate reduction in the damping of the wire motion.

6 Formulation of the Problem

Chapter 6 is based on the results of numerical calculations that I have conducted on MATLAB. I have utilised the Eq.40-43. Moreover, to calculate the trajectories of quasiparticles I have used the MATLAB ode-solver *ode15s* since the equations are stiff ordinary differential equations. For the modelling of heat flux(heat current), we consider quasiparticles with average energy instead of individual energies. We calculated the heat reflection of the flux from the vortex systems as function of time and study the spectral properties of reflection coefficient using MATLAB built in

function *fft(X)* which uses fast Fourier transform algoritm. Code used to run this numerical calculations are given in Appendix A for further reference.

Andreev reflection technique, pioneered at Lancaster is the only method enabling us to diagnose the dynamics of quantized vortices and quantum turbulence in superfluid ^{3}He in the more complicated regime of very low temperatures. However, the result through this technique is indirect. Thus, specific form of reflection and interpretation of the experiments, theoretical and numerical investigation has to be conducted.

Accordingly, we will consider a two-dimensional system of point vortices and study the dynamics of such system numerically using Andreev reflection technique. Two-dimensional system with the vortices of the same polarity can be associated with the system of straight vortices in rotating container. Meanwhile, two-dimensional system with vortices of different polarities is associated with cross cut of the quantum turbulence (chaotic vortex tangle shown in Figure 7) produced by vibrating wire.

This particular approach is based on the fact that the dispersion curve $E = E(\mathbf{p})$ of quasiparticles is fixed to the reference frame of the superfluid so, in a superfluid progressing with velocity $\mathbf{v}_s$, the dispersion curve becomes $E(\mathbf{p}) + \mathbf{p} \cdot \mathbf{v}_s$ where here $\mathbf{p}$ is the momentum [12] [6]. Hence, a side of the vortex line introduce a potential barrier to oncoming quasiparticles, which can be reflected back almost similarly becoming quasiholes; whilst the other side of the vortex lets the quasiparticle to pass through.

This section is referred to the Andreev reflection experiments conducted in the paper *Interaction of ballistic quasiparticles and vortex configurations in superfluid ^{3}He-B*[9]. First of all, it is important for us to know the governing equations of the system. To make everything simple, we will analyse the problem of motion of quasiparticles in the (x, y) plane in the presence of N straight vortex lines aligned in the z direction. Consequently, the kinetic energy of a thermal excitation of momentum $\mathbf{p}$ is measured with respect to the Fermi energy ϵ_F is denoted as

$$\epsilon_p = \frac{p^2}{2m*} - \epsilon_F \tag{26}$$

and here p=$|\mathbf{p}|$. Thus, it is essential to know that the following numerical values are taken at zero bar pressure [37] which are needed to depict the motion of the excitation

Fermi velocity : $v_F \approx 5.48 \times 10^3$ cm/s
Fermi momentum : $p_F = m * v_F \approx 8.28 \times 10^{-}20 gcm/s$
Fermi energy : $\epsilon_F = p_F^2/(2m*) \approx 2.27 \times 10^{-}16 erg$
Effective mass : $m* \approx 3.01m = 1.51 \times 10^{-}23g$ where m is the mass of the ^{3}He atom

Meanwhile, let us denote Δ_0 to be the magnitude of the superfluid energy gap. In the vicinity of the vortex axis, the radial distances r smaller than the zero-temperature coherence length, $\xi_0 = \hbar v_F/\pi\Delta_0 \approx 0.85 \times 10^{-5} cm$ the energy gaps drops to zero and can be proximated by $\Delta(r) \approx \Delta_0 tanh(r/\xi_0)$[5] [32]. Since we are interested in what happens to the excitation when r $\gg \xi_0$, we neglect spatial dependence of energy gap and assume constant value, $\Delta_0 = 1.76 k_B T_c \approx 2.43 \times 10^{-19} erg$, where k_B is Botlzmann's constant and T_c is the critical temperature.

A vortex point is the intersection of each vortex line with the (x, y) plane . Every vortex point moves with the flow field created by all other vortex points. The ith vortex point located at the position $\mathbf{r}_i(t) = x_i(t)\mathbf{i} + y_i(t)\mathbf{j}$ produces the following velocity field at the point $\mathbf{r}$:

$$\mathbf{v}_i(\mathbf{r}, t) = \frac{\kappa_i}{2\pi|\mathbf{r} - \mathbf{r}_i(t)|^2} - \mathbf{i}[y - y_i(t)] + \mathbf{j}[x - x_i(t)] \tag{27}$$

where $\mathbf{r} = x\mathbf{i}+y\mathbf{j}$, and $\mathbf{i}, \mathbf{j}$ are unit vectors along the x and y axes respectively. The circulation κ_i of the ith vortex is $\kappa_i = \pm\kappa$ and the + and - signs denote a vortex and an antivortex respectively such that vortex represents anticlockwise rotation whilst antivortex represent clockwise rotation in the (x, y) plane. The quantity

$$\kappa = \frac{h}{2m} = \frac{\pi\hbar}{m} = 0.662 \times 10^{-3} cm^2/s \tag{28}$$

denote the quantum of circulation in ^{3}He-B. The **velocity field** at point $\mathbf{r}$ created by the N vortices is

$$\mathbf{v}_s(\mathbf{r}, t) = \sum_{i=1}^{i=N} \mathbf{v}_i(\mathbf{r}, t) \tag{29}$$

hence the **velocity of the ith vortex point** $\mathbf{r}_i$is

$$\frac{\mathbf{r}_i(t)}{dt} = \sum_{j=1, j\neq i}^{i=N} \mathbf{v}_j(\mathbf{r}_i). \tag{30}$$

In the presence of vortices the energy of the thermal excitation becomes

$$E = \sqrt{\epsilon_p^2 + \Delta_0^2} + \mathbf{p} \cdot \mathbf{v}_s(\mathbf{r}, t) \tag{31}$$

Referring to Eq.31, the spatial variation in the order parameter is negligible for the sake of simplicity. Moreover, we also presume on a spatial scale which is larger than ξ_0, the interaction term $\mathbf{p} \cdot \mathbf{v}_s$ varies and that the excitation can be considered as a dense object with momentum $\mathbf{p}$=$\mathbf{p}$(t), position $\mathbf{r}$=$\mathbf{r}$(t) and the energy $E = E(\mathbf{p},\mathbf{r}, t)$. Henceforth, we are able to consider Eq.31 as an **effective Hamiltonian** for which the equations of motion are

$$\frac{d\mathbf{r}}{dt} = \frac{\partial E(\mathbf{p},\mathbf{r})}{\partial \mathbf{p}} = \frac{\epsilon_p}{\sqrt{\epsilon_p^2 + \Delta_0^2}} \frac{\mathbf{p}}{m*} + \mathbf{v}_s \tag{32}$$

$$\frac{d\mathbf{p}}{dt} = -\frac{\partial E(\mathbf{p},\mathbf{r})}{\partial \mathbf{r}} = -\frac{\partial}{\partial \mathbf{r}}(\mathbf{p}\cdot\mathbf{v}_s) \tag{33}$$

We will now focus on Eq.32. It corresponds to the group velocity of quasiparticles. When a quasiparticle with momentum $\mathbf{p} < \mathbf{p_F}$ moves toward the increasing potential represented by $\mathbf{p}\cdot\mathbf{v}_s$, the momentum decreases. Therefore, quasiparticle with energy ϵ_p, for $\epsilon_p > 0$, then $\epsilon_P \to 0$. When $\mathbf{p}$ pass the value $\mathbf{p_F}$, hence ϵ_P changes sign and becomes negative such that $\epsilon_P < 0$. Consequently, we now have quasihole, since based on Eq.32 in the first term, direction of momentum $\mathbf{p}$ is the same and thus the whole term changes sign and the velocity of the excitation is reversed. Hence, the thermal excitation is reflected back on the same path without exchanging of momentum which is always in the vicinity of Fermi momentum. Therefore, this theoretically explains Andreev reflection.

Quasiparticles are excitations of energy $\epsilon_p > 0$ while quasiholes are denoted by energy $\epsilon_p < 0$. The right-hand side of Eq.33 is the force acting on the excitation.

For the sake of simplicity, it is convenient to first rewrite both Eq.32 and Eq.33 in dimensionless form. We introduce the dimensionless variables as follows:

$$H = \frac{E}{\Delta_0} \tag{34}$$

$$\mathbf{\Pi} = \frac{\mathbf{p}}{p_F} \tag{35}$$

$$\mathbf{V}_s = \frac{\xi_0}{\kappa}\mathbf{v_s} \tag{36}$$

$$\mathbf{R} = (X,Y) = \left(\frac{x}{\xi_0}, \frac{y}{\xi_0}\right) = \frac{\mathbf{r}}{\xi_0} \tag{37}$$

$$\tau = t/t_0 \tag{38}$$

where $t_0 = \xi_0 p_F/\Delta_0 = 2.9 \times 10^{-6}$s. The Hamiltonian Eq.31, and the equations of motion from Eq.32 and Eq.33, then become

$$H(\mathbf{\Pi},\mathbf{R},\tau) = \lambda \sqrt{(\mathbf{\Pi}^2 - 1)^2 + \lambda^{-2}} + \frac{m*}{m}\pi^2 \mathbf{\Pi}\cdot\mathbf{V}_s(\mathbf{R},\tau) \tag{39}$$

and

$$\frac{dX}{d\tau} = \lambda \frac{2(\Pi^2 - 1)}{\sqrt{(\Pi^2 - 1)^2 + \lambda^{-2}}} \Pi_x + \frac{m*}{m} \pi^2 V_{sx}(\mathbf{R}, \tau) \tag{40}$$

$$\frac{dY}{d\tau} = \lambda \frac{2(\Pi^2 - 1)}{\sqrt{(\Pi^2 - 1)^2 + \lambda^{-2}}} \Pi_y + \frac{m*}{m} \pi^2 V_{sy}(\mathbf{R}, \tau) \tag{41}$$

$$\frac{\Pi_x}{d\tau} = -\frac{m*}{m} \pi^2 \left(\Pi_x \frac{dV_{sx}}{dX} + \Pi_y \frac{dV_{sy}}{dX} \right) \tag{42}$$

$$\frac{\Pi_y}{d\tau} = -\frac{m*}{m} \pi^2 \left(\Pi_x \frac{dV_{sx}}{dY} + \Pi_y \frac{dV_{sy}}{dY} \right) \tag{43}$$

where the dimensionless parameter λ is

$$\lambda = \frac{\epsilon_F}{\Delta_0}. \tag{44}$$

We shall assume the value $\lambda = 1 \times 10^3$ in our numerical computation. Lastly, the dimensionless superfluid velocity is

$$\mathbf{V}_s(\mathbf{R}, \tau) = \sum_{i=1}^{i=N} \mathbf{V}_i(\mathbf{R}, \tau = \sum_{i=1}^{i=N} \frac{\Gamma_i}{2\pi |\mathbf{R} - \mathbf{R}_i(\tau)|^2} \times -\mathbf{i}[Y - Y_i(\tau)] + \mathbf{j}[\mathbf{X} - \mathbf{X_i}(\tau)] \tag{45}$$

where Γ_i=1 for vortices, Γ_i = -1 for antivortices and

$$\frac{d\mathbf{R}_i(\tau)}{d\tau} = \sum_{j=1, j \neq i}^{j=N} \mathbf{V_j}(\mathbf{R_i}) \tag{46}$$

.

6.1 Heat Transport through the Velocity Field of a Vortex

This section is based on the article *Ballistic Propagation of Thermal Excitation Near a Vortex in Superfluid ^{3}He-B* [8]. The vortex tangle in a superfluid turbulence in ^{3}He at ultralow temperatures is studied by the detection of the fraction of quasiparticles which are Andreev reflected by the vortices and measuring the heat which is transported by the quasiparticles. As discussed in previous sections, quasiparticles characterized by the particular impact parameter ρ_0 are Andreev reflected by the vortex if their energies satisfy the condition

$$\Delta_0 \leq E \leq \Delta_0(1 + 3\pi\xi_0/2\rho_0) \tag{47}$$

If this condition is not fulfilled, the quasiparticles are able to pass freely across the vortex velocity field. If the system which consists of the vortex and quasiparticles is in thermal equilibrium, there is no preferred direction around the vortex. Incident and transmitted fluxes at one side of the vortex cancel out by the fluxes in

the opposite direction, and no net flow of energy exists when the value of temperature is constant everywhere around the vortex.

Results of a net flux of quasiparticles and energy exist only if there is some small temperature difference, $\delta T \ll T$ between both sides. If this case takes place, the heat carried by the incident quasiparticles is described by the equation

$$\delta Q_{inc} = \int_{\Delta_0}^{\infty} N(E) v_g(E) E \frac{\partial f(E)}{\partial T} \delta T dE \tag{48}$$

where

$$N(E) = N_F \frac{E}{(E^2 - \Delta^2)^{1/2}} \tag{49}$$

here

$$N_F = \frac{m p_F}{\pi^2 \hbar^3} \tag{50}$$

denotes the density of states at the Fermi energy with the corresponding Fermi momentum p_F. The group velocity of a Bogoliubov (broken Cooper pair) quasiparticles v_g is given by the expression

$$v_g = \frac{\epsilon_p}{E} v_F = \frac{(E^2 - \Delta^2)^{1/2}}{E} v_F \tag{51}$$

and $f(E)$ is the Fermi distribution function, which, at ultralow temperatures is transformed into the Boltzmann distribution and describes the mean occupation number of a state with energy E :

$$f(E) = e^{-\frac{E}{k_B T}} \tag{52}$$

The thermal flux of quasiparticles incident on the vortex velocity per unit length per unit time is obtained with the help of Eq.49, 51 and 52 which is described by the expression

$$\delta Q_{inc} = N_F v_F \frac{\delta T}{k_B T^2} \int_{\Delta}^{\infty} E^2 e^{-\frac{E}{k_B T}} dE \approx N_F v_F \Delta_0^2 \frac{\delta T}{T} e^{-\frac{\Delta_0}{k_B T}} \tag{53}$$

The total heat current incident on the vortex per unit time in a plane current of quasiparticles with transverse cross section R_0 is

$$Q_{inc} = 2R_0 \delta Q_{inc} = 2R_0 N_F v_F \Delta_0^2 \frac{\delta T}{T} e^{-\frac{\Delta_0}{k_B T}} \tag{54}$$

Now, we assume that in the (x,y) plane perpendicular to the straight vortex line, the polarity of the vortex located at (0,0) is positive and we also consider incoming

quasiparticles in the positive x direction. In this case,there are two regions affected :

(i) The upper half plane will certainly be transparent for quasiparticles so that the heat transferred by quasiparticles through this half plane will meet no obstruction.
(ii) The lower half plane of vortex flow field will reflect a fraction of quasiparticles and induce some thermal resistance.

A quasiparticle with the impact parameter ρ_0 is transmitted through the vortex velocity field if it carries energy $E > \Delta_0(1 + \frac{3}{2}\pi\xi_0/\rho_0)$ and thus the heat which is transferred per unit time by such a quasiparticle can be calculated as

$$\begin{aligned}\delta Q(\rho) &= \int_{\Delta(1+\frac{3\pi\xi_0}{2\rho_o})}^{\infty} N(E)v_g(E)E\frac{\partial f(E)}{\partial T}\delta T dE \\ &\simeq Q_{inc}\frac{1}{2R_0}(1+\frac{3\pi\xi_0}{\rho_0})e^{-(\frac{\Delta_0}{k_BT})(\frac{3\pi\xi_0}{2\rho_0})}\end{aligned} \tag{55}$$

and by estimating the ratio $\frac{\xi_0}{\rho_0}$ we only kept the linear term.

The total amount of energy transferred through the vortex by quasiparticles originated within the interval $R_0 \leq y \leq R_0$ is

$$Q_{tr} = \frac{Q_{inc}}{2}[1 + \frac{1}{R_0}\int_0^{R_0}(1+\frac{3\pi\xi_0}{\rho_0})e^{-(\frac{\Delta_0}{k_BT})(\frac{3\pi\xi_0}{2\rho_0})}d\rho_0] \tag{56}$$

The integral in Eq.56 can be estimated as

$$\approx R_0 e^{-(\frac{\Delta_0}{k_BT})(\frac{3\pi\xi_0}{2\rho_0})} \tag{57}$$

Hence the fraction of heat which is transferred through the velocity field of the vortex is

$$\delta f_{tr} = \frac{1}{2}(1 + e^{-(\frac{\Delta_0}{k_BT})(\frac{3\pi\xi_0}{2\rho_0})} \tag{58}$$

In experiments at ultralow temperatures we have $\Delta_0/k_BT \sim 10$ and thus the cross section of the thermal flux is $R_0 \sim 10\xi_0$ and the total heat transferred through the vortex is approximately 52%. If the heat has cross section $\sim 10^2\xi_0$, the fraction of the heat transferred is approximately 0.82. Therefore, the reflection of the heat flux occurs only in the close vicinity of the vortex core.

Based on the article *Two-dimensional model of interactions between thermal quasiparticles and turbulent structures in* $^3He - B$ [26], the trajectory of quasiparticles was found by numerical solution :

$$\dot{\mathbf{R}} = \frac{2\lambda(\Pi^2-1)}{\sqrt{(\Pi^2-1)^2+\lambda(-2)}}\mathbf{\Pi} + \frac{m^*}{m}\pi^2\mathbf{V}_s(\mathbf{R},\tau) \tag{59}$$

$$\dot{\mathbf{\Pi}} = -m^* m^{-1} \pi^2 \nabla(\mathbf{\Pi} \cdot \mathbf{V}_s(\mathbf{R}, \tau)) \tag{60}$$

for random initial energies (momenta) and directions of motion. Therefore, having identified the trajectories of the quasiparticles that are Andreev reflected (as quasiholes) by the vortex gas or a gas of vortex-antivortex pairs, for a particular realisation R, of the initial configuration of the vortex gas the reflection coefficient is then calculated as

$$f_r^R = \frac{1}{q_0} \sum_{j=1}^{K} \alpha_i H_{i0} \quad with \quad q_0 = \sum_{j=1}^{K} H_{i0} \tag{61}$$

where α_j=1 if the j-th-quasiparticle is reflected, otherwise α_j=0.

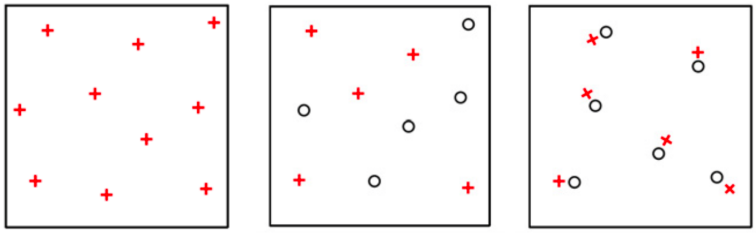

Figure 14: *Zoomed view of configurations (1)left (2)center (3)right; +(red) represents vortices whilst ◯ represents antivortices.[26]*

The coefficient reflection, f_r as a function of the total number of vortices,N in the system is shown in Figure 15. It can be observed from this figure, in all cases the reflection coefficient increases with the total density of vortex points. The reflection coefficients in the system (1) of vortices of the same polarity and in the vortex gas (2) with zero net circulation are close, although in (2) the partial screening seems to have a slightly bigger effect. For both these configurations, the behavior of the reflection coefficient with the total number of vortex points obeys the same power law, f_r $N^{3/4}$. Hence, it points itself to a presence of partial screening in a statistically uniform, random system of vortices such as either in (1) or (2).

Certainly, in the absence of partial screening the ensemble average reflection coefficient would be proportional to the total number of vortex points, N. Meanwhile, in the case where the vortices of opposite polarities form pairs ("rings"), partial screening possess more pronounced role and the reflection coefficient falls by almost a factor of 2. For the gas of vortex-antivortex pairs, the nature of the reflection coefficient with the total number of vortex points seems to be sufficiently close to the power law f_r $N^{0.9}$. This is because the configuration (3) the screening takes place mostly within or in the close vicinity of each pair. At distances larger that d from each pair the flow field is close to that of a vortex dipole. For incoming quasiparticles, such a flow field presents much weaker potential barrier than that of a single, isolated vortex. Thus, the average reflection coefficient should be nearly proportional to the number of vortex pair, $N/2$.

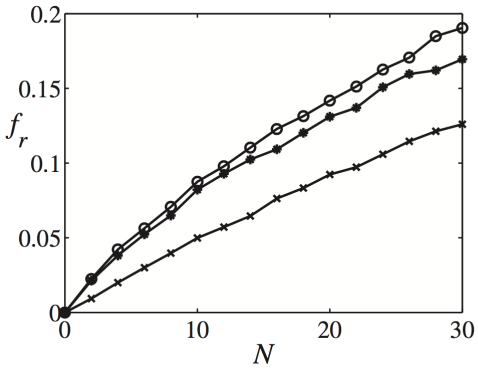

Figure 15: *Reflection coefficient as a function of the total number of vortex point.Lines from top to bottom, correspond to configurations (1),(2) and the gas of vortex-antivortex pairs (3). [26]*

Single Vortex

In the case of a single vortex, most generally used differential equation solvers are not ideal since they failed to conserve the total energy and total angular momentum of the quasiparticle by large amounts (≥ 10 %). However, in the case of more complex time-dependent vortex configurations, energy and momentum of quasiparticles are not conserved but certainly have doubts about our results since the basic conservation laws were not satisfied in the simplest case of a single vortex.

The best way to approach this problem is to build the conservation law into the numerical scheme and the numerical method must be symplectic and conserve phase-space volume.[25] Unfortunately, there are a couple problems arise from this method (mainly in context of gravity) :

(i) Hamiltonian has the additive form $H = T(\mathbf{p}) + V(\mathbf{q})$ where $\mathbf{p}$ and $\mathbf{q}$ are the generalized momenta and positions respectively , T is the kinetic energy and V the potential energy. Henceforth, this is problematic since $\mathbf{p}$ and $\mathbf{q}$ appear in non-linear combinations.
(ii) Next problem is the stiffness of our equations of motion, as very rapid time scale appear at the Andreev turning points.

Nevertheless, it has been found that we can solve the governing equations with satisfactory accuracy using the MATLAB code *ode*15*s* which is a quasiconstant step size implementation of the numerical differentiation formulas (NDF) specifically efficient for solving stiff problems(detailed description of *ode*15*s* MATLAB solver and corresponding software refer [27]). Error tolerances were lowered until particle trajectory had sufficiently converged, in particular at reflections when solving Eq.40-43. In this section, the system occurs in an environment where the positive side is absolutely transparent, thus there is no barrier whilst on the negative side when the energy of the particle is not high enough then the quasiparticle is Andreev reflected.

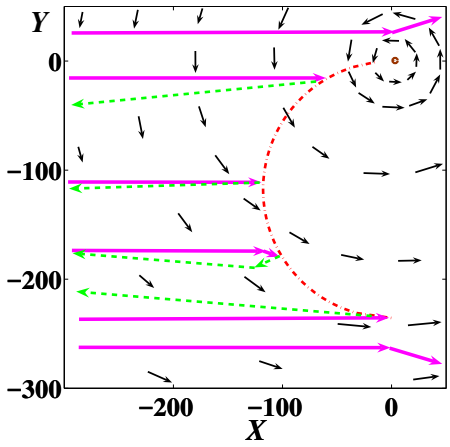

Figure 16: *Illustration shows the trajectories of excitations for different values of* Y_0 *in the presence on a single vortex at the origin. The superfluid velocity is indicated by arrows, quasiparticles trajectories are solid purple lines, quasiholes trajectories are dashed green lines. The dashed dotted red curve denotes locus of Andreev reflection.*

The velocity field of the vortex is

$$\mathbf{V}_s(\mathbf{R}) = \frac{1}{2\pi R^2}(-\mathbf{i}Y + \mathbf{j}X) \tag{62}$$

Since the vortex is stationary,this velocity field is time independent and the governing Eq.40-43 have two integrals of motion:

(i)the energy define by Hamiltonian Eq.39
(ii)the z component of the angular momentum which is

$$J = \Pi_y X - \Pi_x Y \tag{63}$$

Now, we will examine the behavior of a single vortex in 2-Dimensional (x, y) plane given the initial conditions at τ=0, initial momentum, $\mathbf{\Pi}_0 = (1.0001, 0)$ and corresponds to a quasiparticle moving in the x direction with energy $E = \Delta_0 + k_B T$ for given temperature $T \approx 0.1T_c$. The initial position is (X_0, Y_0) with $X_0 = -1 \times 10^4$ far away from the vortex. We analyse the trajectory of the quasiparticle as a function of Y_0, which plays the role of impact parameter. We will observe three cases :

(i)$Y_0 \geq 0$

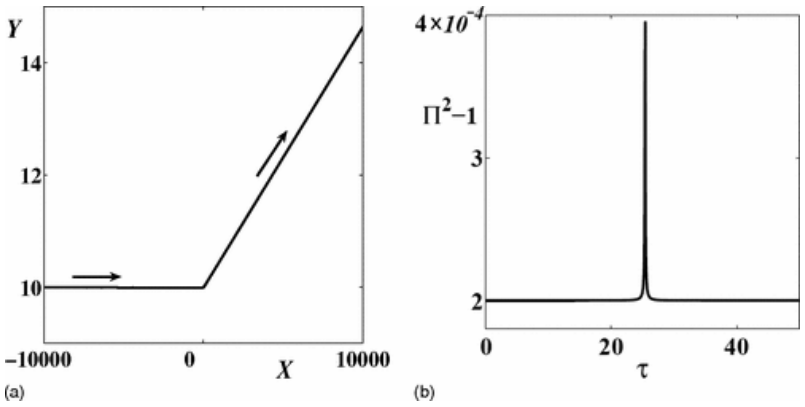

Figure 17: (a) *Trajectory of quasiparticle in the presence of a single anticlockwise vortex at origin.Arrows indicate direction of motion. (b) Plot of* $\Pi^2 - 1$ *vs time* τ *corresponding to (a) and note that the quasiparticle remains a quasiparticle*

Here, we have no reflection. For instance, in Figure 17(left) shows the quasiparticle's trajectory for Y_0=0 whilst Figure 17(right) shows that $\mathbf{\Pi}^2 - 1$ remains positive at all times τ, denoting that the quasiparticle retains its nature.

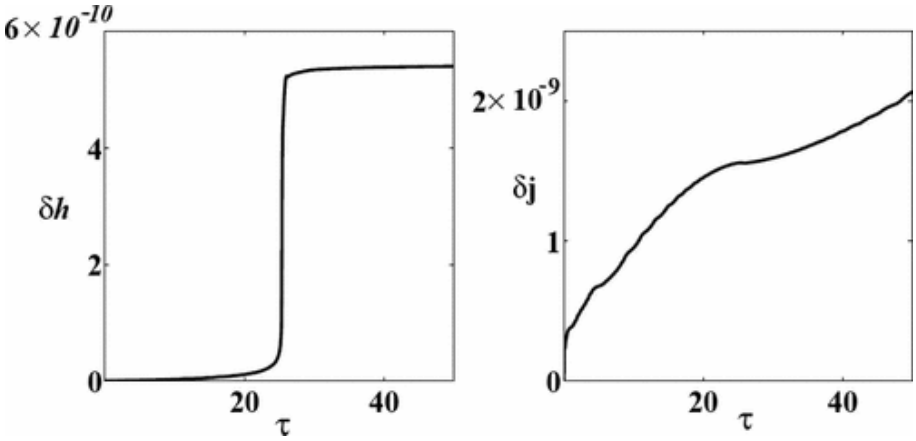

Figure 18: *Diagram represents plot of relative energy variation* $\delta h = (H - H_0)/H_0$ *vs time* τ *(left) and relative angular momentum variation* $\delta j = (J - J_0)/J_0$*(right) corresponding to Figure 17.*

Figure 18 verifies that our numerical method conserves energy and angular momentum very well. The left hand side of Figure 18 represents that the relative error in the energy, $\delta h(\tau) = [H(\tau) - H_0]/H_0$, where H_0 denotes the initial energy and is less than 6×10^{-10} whilst the right hand side of the figure shows the relative error in computing the angular momentum, $\delta j(\tau) = [J(\tau) - J_0]/J_0$ where J_0 denotes the initial angular momentum; is less than 2.5×10^{-9}.

(ii)$Y_0 < 0$

For $|Y_0|$ is not too large, the incident quasiparticle is Andreev reflected as shown for example in Figure 19 (left) for Y_0 = -10. The figure on the right shows that $\mathbf{\Pi}^2 - 1$ changes sign, thus proving that, upon reflection, the quasiparticles become

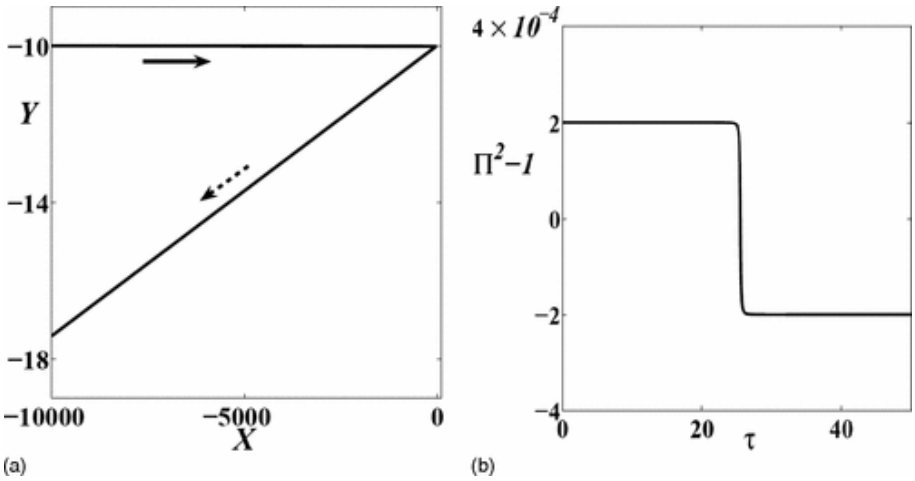

Figure 19: *(a) Trajectory of quasiparticle in the presence of a single anticlockwise vortex at the origin. Arrows indicate the direction of motion. Right: Plot of* $\Pi^2 - 1$ *vs time* τ *corresponding to (a), note quasiparticle becomes a quasihole.*

quasihole. In this computation, the numerical errors in conserving energy and angular momentum are $\delta h < 8 \times 10^{-10}$ and $\delta j < 2 \times 10^{-9}$, respectively. Figure 19 shows another Andreev reflection but for $Y_0 = -205$. Consequently, if Y_0 the incident quasiparticle is Andreev reflected; the dashed-dotted red curve in Figure 16 marks the path of the quasiparticle. It is apparent that there is a maximum value of $|Y_0|$, past which the quasiparticle with energy ϵ_p is not Andreev reflected; this value which is denoted in dimensionless units is approximately equal to $S_0 = 3\pi(\Delta_0/\epsilon_p)^2 \approx 269$ where we used the value $\epsilon_p = \epsilon_F(\mathbf{\Pi}^2 - 1) \approx .00002\epsilon_F$ for $\mathbf{\Pi} = 1.0001$. Henceforth, $S_0 = 269$ is the (dimensionless) Andreev shadow of a single vortex to quasiparticles of that particular (dimensionless) momentum Π.

(iii)0 > -S > Y_0
The quasiparticle's trajectory is deflected by the vortex but remains a quasiparticle.

Vortex-vortex pair

In the case of velocity field of two vortices , it is time dependent and therefore the Hamiltonian of the thermal thermal excitation has no integrals of motion. In contrast with the previous case of a single vortex, H and J are not conserved. The only quantity which is constant is the distance between the vortices. There are two cases to consider :

(i)two vortices of the same circulation (vortex-vortex pair)
(ii)two vortices of the opposite circulations (vortex-antivortex pair)
In this section, we will focus on the first case. Two vortices of the same circulation at distance d from one another rotate around a point halfway between them with velocity

$$v_{rot} = \frac{\kappa}{2\pi d} \tag{64}$$

In dimensionless variables we have that

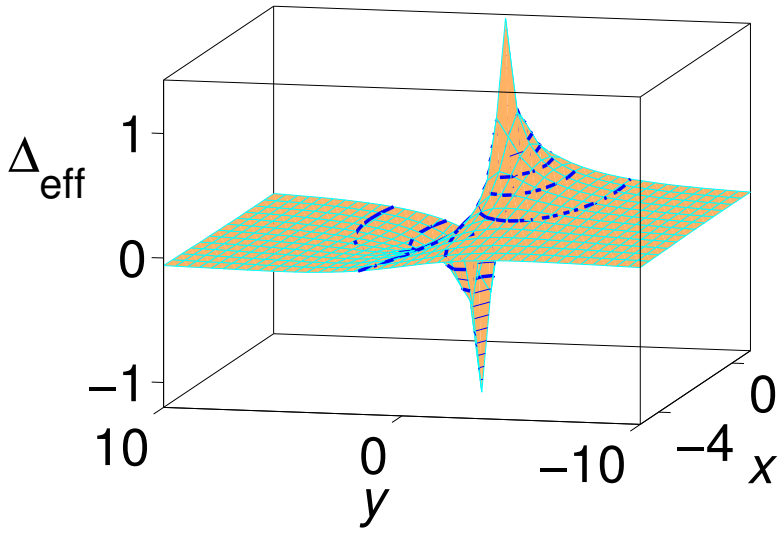

Figure 20: *Diagram shows the effective potential felt by the quasiparticles propagating in the velocity field of a single vortex. There is no barrier on the right side of the vortex leading to quasiparticles passing freely. However, on the left side there is a barrier and quasiparticles are Andreev reflected as quasiholes.*

$$V_{rot} = \frac{1}{2\pi D}, \quad D = \frac{d}{\xi_0} \tag{65}$$

Far from the vortices, the velocity of the quasiparticle can be estimated from Eqs.40 and 41

$$\frac{d\mathbf{R}}{d\tau} \approx 2\lambda^2(\Pi^2 - 1)\mathbf{\Pi} \tag{66}$$

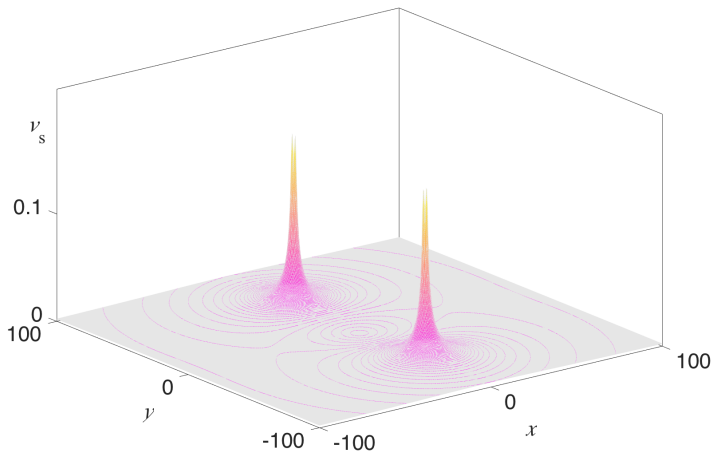

Figure 21: *Velocity field of two vortices*

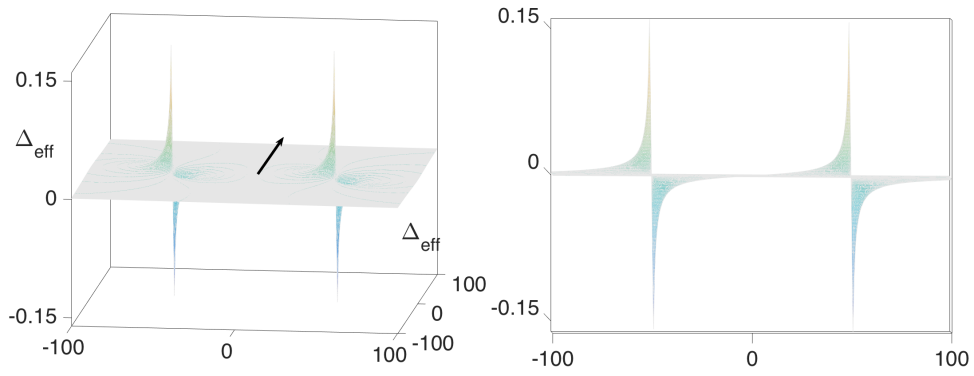

Figure 22: *Effective potential created by 2 vortices. Figure on the right shows the effective potential produced from a different angle. Quasiparticles pass perpendicular to both the vortices.*

Referring to Figure 23(right) and Figure 20,the effective potential produced are similar. Thus, for quasiparticles moving in a parallel direction to the two vortices, they experience the same effective potential produced by a single vortex. In conclusion, the motion of quasiparticles passing through any vortices is important in order to determine its progress at a later time.

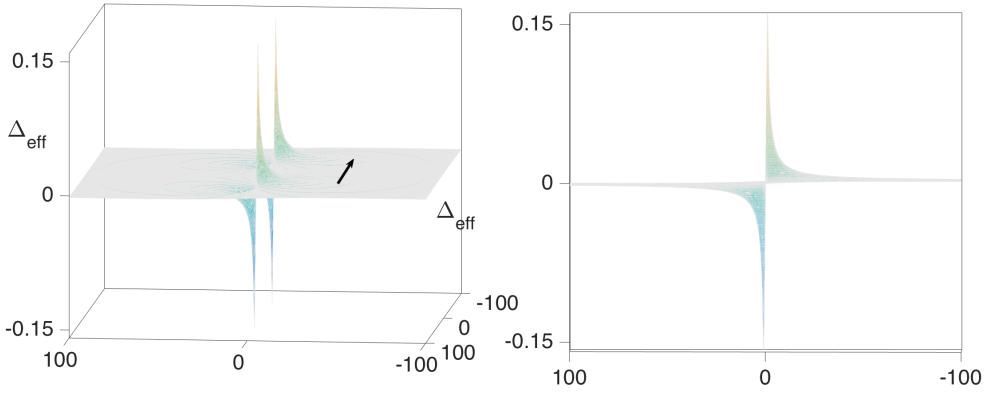

Figure 23: *Effective potential created by 2 vortices felt by quasiparticles. Diagram on the right shows the effective potential produced from a different angle.*

Vortex-Antivortex Pair

A vortex and antivortex , set at distance D from each other, move through the fluid with (dimensionless) translational velocity

$$V_{tran} = \frac{1}{2\pi D}, \quad D = \frac{d}{\xi_0} \tag{67}$$

We will now consider two cases :

(i) vortex-antivortex pair and the quasiparticle move in the same direction
(ii) vortex-antivortex pair and the quasiparticle move in the opposite directions.

Through experiments conducted as stated in [9], the total shadow, $S_1 + S_2$ of the vortex configuration is greatly reduced in case (ii). In both cases, during the time scale of the circulation, vortex pair only moves by 0.01. Henceforth, we can conclude that the relative motion of vortices and excitations has a strong effect on the shadow.

Now, we will analyse the dependence of the Andreev reflection on D. First of all, we consider the case in which quasiparticle and vortex pair move in the same direction. When D is reduced, the total shadow increases and at a certain value of D the shadows will merge into one single shadow. However, upon further reduction of D, total shadow decreases.

Next will be the second case in which the vortex-antivortex pair and the quasiparticle move in the opposite directions. Independent of D, the total shadow of a vortex pair traveling in the opposite direction of the quasiparticles is about half that of a vortex pair traveling in the same direction. Nevertheless, the shadow of the vortex-antivortex pair also depends on the angle α between the direction of propagation of the quasiparticle and the direction of motion of the vortex-antivortex pair.

Many vortices

For a system with three vortices and more, it will be in a chaotic state and it is more complicated to study this case. Hence, numerical modeling is used to observe this vortex system.

6.2 Spectral properties of reflection coefficient

We have conducted numerical experiments in the presence of two and three vortices of the same polarity. The time we run the experiments was up to 10^6 in units of Eq.35-38. We recorded the heat reflection coefficient as function of time and study its spectral properties. Then we analyse the spectral property to make analogy with the dynamics of vortices.

Figure 24 demonstrates the three vortex system for different time moments. It can be seen that there is a small change in the movement of vortices. However, for a system of two vortices of the same polarity they will only move in a circular motion.

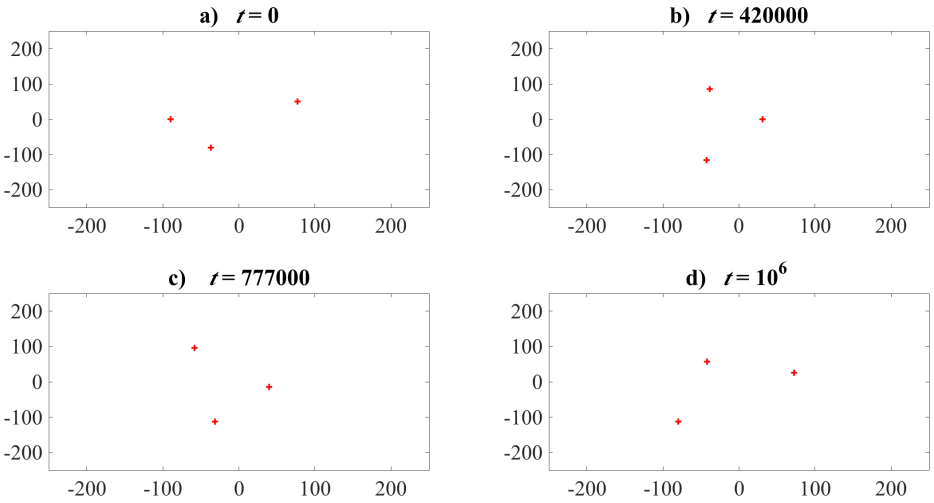

Figure 24: *Diagram shows the snapshots of the system of three vortices of the same polarity for different time moments and is a demonstration of dynamics of the vortex system*

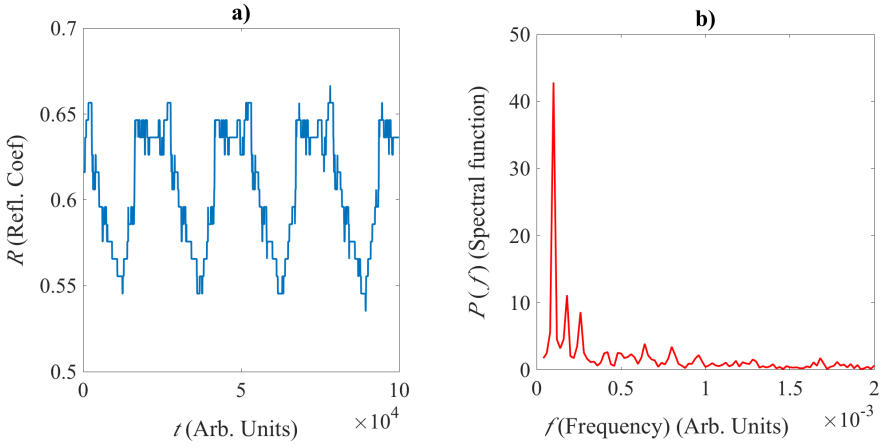

Figure 25: *Figure shows the reflective spectrum of 2 vortices. Figure a) is a graph time against reflective coefficients,R and figure b) is frequency against spectral function*

Figure 25(left) illustrates the reflective coefficients of quasiparticles. As seen on the graph, it is periodic for arbitrary units of time. This corresponds to the two vortices of the same polarity moving in a circular motion. However, our result is not smooth because of time discretization and also our experiment was set in a small box in order to save computer time when running the codes. Figure 25(right) is the Fourier Transform of the figure on the left.

The spectral function,$P(f)$ is :

$$P(f) = \int R(t)e^{-iwt}dt \tag{68}$$

The frequency is represented by :

$$f = \frac{1}{\pi D^2}$$

and our calculated frequency is $f \sim 1.09 \times 10^{-}4$, with D the distance betweeen two vortices and D=54.

From the graph, we could see that at the peak of the spectral function, we can observe the dominating frequency in the system. The frequency obtained is

$$f \sim 1.02 \times 10^{-}4$$

Thus, our calculated frequency and the frequency obtained from our experiment is very close. Hence, our estimation is proven to be quite accurate. The rest of the frequency is just discretization. This is the result of the quasiparticles not being sufficiently close and the time set to run the code is not small. The time set is again to save computer time and the use of a home laptop which is not powerful enough to run big data. The graph is not really sinusoidal because of the degree of discretization is rough.

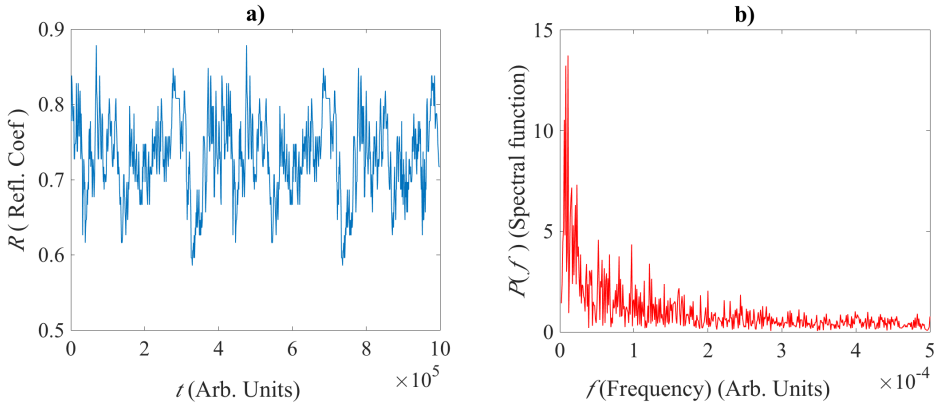

Figure 26: *Figure above shows the reflective spectrum of 3 vortices of the same polarity(anticlockwise). Figure a) is a graph time against reflective coefficients,R and figure b) is frequency against spectral function*

From Figure 26 a) the reflective coefficients are not smooth and not mono periodic. However, for Figure 26 b) we consider the average distance between the three vortices, and the calculated peak frequency is around $1.02 \times 10^{-5} - 1.20 \times 10^{-5}$ whilst the experimental value is around $0.9 \times 10^{-5} - 1.5 \times 10^{-5}$. This is because as

seen in Figure 24 the distance of vortices do not have a big change in different time moments.

Therefore, to make our result more precise and our graphs smoother, there are a few steps we could do :

(i) increase time integral by more than twice
(ii) decrease time steps
(iii) decrease initial position of quasiparticles

Conclusion

In conclusion, according to the spectral analysis of reflection coefficient we are able to get the information about distances and velocities of vortices in the system. The results and findings obtained are able to facilitate in a better understanding of experiments and their interpretations. For example, we have managed to find the effective potential felt by quasiparticles from moving vortex system. Henceforth, our findings have even shown us that in a system of two vortices quasiparticles moving parallel to the line connecting the cortex cores could feel the effective potential produced by one vortex instead. Therefore, it is impressive to see how mathematical modeling could show us how a superfluid system works in real life through the numerical implementation of theory using MATLAB but still obtain the same outcome as an experiment run in the lab.

Consequently, from the numerical outcomes, the total Andreev shadow is not necessarily the sum of the shadows of individual vortices and does not mainly depend on the distance but also on the relative orientation between quasiparticles and vortex motion. It is possible that the interpretation of the outcome is caused by the partial screening effects being averaged out.

Moreover, the spectral analysis, which has never been performed before, allows us to follow the dynamics of vortices evolved in time and find average quantities, such as mean intervortex distances, frequencies and velocities dominating in the system. There is great correspondence between the peaks of the spectral function and the numerically calculated velocities (angular velocities) of vortices through our analysis.

References

[1] Banerjee Abhishek. *Superfluid Helium Climbs Up Walls SUPERFLUID HELIUM DEFIES GRAVITY.*

[2] J B. Ketterson. The microscopic theory of superconductivity: Cooper pairing and the bardeen–cooper–schrieffer theory, 09 2016.

[3] R. Balian and N. R. Werthamer. Superconductivity with pairs in a relative p wave. *Phys. Rev.*, 131:1553–1564, Aug 1963.

[4] Sebastien Balibar. The discovery of superfluidity.

[5] John Bardeen, R. Kümmel, A. E. Jacobs, and L. Tewordt. Structure of vortex lines in pure superconductors. *Phys. Rev.*, 187:556–569, Nov 1969.

[6] 1953 Barenghi, C. F. (Carlo F.), Yuri A Sergeev, and International Centre for Mechanical Sciences. *Vortices and turbulence at very low temperatures.* Wien ; New York : Springer, 2008. Includes bibliographical references.

[7] C. F. Barenghi, R. J. Donnelly, and W. F. Vinen. Friction on quantized vortices in helium ii. a review. *Journal of Low Temperature Physics*, 52(3):189–247, Aug 1983.

[8] C. F. Barenghi, Y. A. Sergeev, and N. Suramlishvili. Ballistic propagation of thermal excitations near a vortex in superfluid ^{3}He−B. *Phys. Rev. B*, 77:104512, Mar 2008.

[9] C. F. Barenghi, Y. A. Sergeev, N. Suramlishvili, and P. J. van Dijk. Interaction of ballistic quasiparticles and vortex configurations in superfluid ^{3}He-B. *Phys. Rev. B*, 79:024508, Jan 2009.

[10] Carlo F. Barenghi, Ladislav Skrbek, and Katepalli R. Sreenivasan. Introduction to quantum turbulence. *Proceedings of the National Academy of Sciences*, 111(Supplement 1):4647–4652, 2014.

[11] C.F. Barenghi, R.J. Donnelly, and W.F. Vinen. *Quantized Vortex Dynamics and Superfluid Turbulence.* Lecture Notes in Physics. Springer Berlin Heidelberg, 2001.

[12] D. I. Bradley, S. N. Fisher, A. M. Guénault, M. R. Lowe, G. R. Pickett, A. Rahm, and R. C. V. Whitehead. Quantum turbulence in superfluid ^{3}He illuminated by a beam of quasiparticle excitations. *Phys. Rev. Lett.*, 93:235302, Dec 2004.

[13] Peter Davidson and P. Davidson. *Turbulence: An Introduction for Scientists and Engineers.* Oxford University Press, 2 edition, June 2015.

[14] Russell J Donnelly. *Quantized vortices in helium II / Russell J. Donnelly.* Cambridge studies in low temperature physics ; 3. Cambridge University Press, Cambridge, 1991.

[15] Shaun N. Fisher. *Turbulence Experiments in Superfluid He-3 at Very Low Temperatures.*, pages 177–257. CISM International Centre for Mechanical Sciences. Springer, 501 edition, 2008.

[16] S.N. Fisher and G.R. Pickett. *Progress in Low Temperature Physics, Chapter 3 Quantum Turbulence in Superfluid 3He at Very Low Temperatures*. Elsevier, 2009.

[17] Gabriele Giuliani and Giovanni Vignale. *Quantum Theory of the Electron Liquid*. Cambridge University Press, 2005.

[18] Landau and Lifshitz. *Fluid Mechanics: Landau and Lifshitz: Course of Theoretical Physics*, volume 6. Elsevier, 2,revised edition, 2013.

[19] L. Landau. Theory of the superfluidity of helium ii. *Phys. Rev.*, 60:356–358, Aug 1941.

[20] A. J. Leggett. Quantum liquids. *Science*, 319(5867):1203–1205, 2008.

[21] Peter V. E. McClintock. Superfluid 3he at zero pressure. *Nature*, 252(5483):441–442, 12 1974.

[22] Edited by Fir0002 NASA Langley Research Center (NASA-LaRC). *Wake Vortex Study at Wallops Island*, 4 May 1990.

[23] Feynman RP. *Application of quantum mechanics to liquid helium. In: Gorter CJ (ed) Progress in low temperature physics*, volume 1. North Holland, Amsterdam, 1955.

[24] P. G. Saffman. *Fundamental properties of vorticity*, pages 1–19. Cambridge Monographs on Mechanics. Cambridge University Press, 1993.

[25] J. M Sanz-Serna and M. P Calvo. *Numerical Hamiltonian problems*. London, New York, Chapman and Hall, 1st ed edition, 1994. Includes indexes.

[26] Y. A. Sergeev, C. F. Barenghi, N. Suramlishvili, and P. J. van Dijk. Two-dimensional model of interactions between thermal quasiparticles and turbulent structures in 3 he-b. *EPL (Europhysics Letters)*, 90(5):56003, 2010.

[27] Lawrence F. Shampine and Mark W. Reichelt. The matlab ode suite. *SIAM Journal on Scientific Computing*, 18(1):1–22, 1997.

[28] R. F. Streater and A. S. Wightman. Pct spin and statistics and all that. 1964.

[29] Erkki Thuneberg. *Helium, Researh on helium in LTL/Helsinki University of Technology*, 19 August 2003.

[30] L. TISZA. Transport phenomena in helium ii. *Nature*, 141:913 EP –, 05 1938.

[31] V. Tsepelin, A. W. Baggaley, Y. A. Sergeev, C. F. Barenghi, S. N. Fisher, G. R. Pickett, M. J. Jackson, and N. Suramlishvili. Visualization of quantum turbulence in superfluid ^{3}He$-b$: Combined numerical and experimental study of andreev reflection. *Phys. Rev. B*, 96:054510, Aug 2017.

[32] T. (Toshihiko) Tsunetō. *Superconductivity and superfluidity*. New York : Cambridge University Press, 1998. Originally published in Japanese.

[33] W F Vinen. How is turbulent energy dissipated in a superfluid? *Journal of Physics: Condensed Matter*, 17(45):S3231, 2005.

[34] W. F. Vinen, Makoto Tsubota, and Akira Mitani. Kelvin-wave cascade on a vortex in superfluid ^{4}He at a very low temperature. *Phys. Rev. Lett.*, 91:135301, Sep 2003.

[35] William F. Vinen and Ladislav Skrbek. Quantum turbulence generated by oscillating structures. *Proceedings of the National Academy of Sciences*, 111(Supplement 1):4699–4706, 2014.

[36] Vollhardt.D. and Wölfle. Peter. *The superfluid phases of helium 3/Dieter Vollhardt, Peter Wölfle*. London, 1990.

[37] John C. Wheatley. Experimental properties of superfluid ^{3}He. *Rev. Mod. Phys.*, 47:415–470, Apr 1975.

A Appendix A

Below are the codes used to run the experiments in Chapter 6.

Listings

Listing 1: This is the code to compute the ordinary differential equation

```
function ds = odefun(t,s,kappa,ksi,Q);

% Defines RHS of the equation describing qusiparticle dynamics

N=length(kappa);        % Number of vortices
s=s(:);
p2=s(3)^2+s(4)^2;  % squared momentum of quasiparticle
Eps=sqrt((p2-1)^2+1/ksi^2); % energy of quasiparticle
J=[[0,1];[-1,0]]; %helper matrix

% Compute v, and dvdq
v=zeros(2,1);
dvdq=zeros(2,2);
for ii=1:N;
    q=s(1:2)-s(4+2*(ii-1)+1:4+2*(ii-1)+2);
    q2=q'*q;
    vi=-kappa(ii)/2/pi*J*q;
    if q2>Q^2;
        vi=vi/q2;
        dvidq=kappa(ii)/pi/q2^2*[[q(1)*q(2),q(2)^2];[-q(1)^2,-q(1)*q(2)]]-kappa(ii)/2/pi/q2*J;
    else    % Solid body rotation
        vi=vi/Q^2;
        dvidq=-kappa(ii)/2/pi/Q^2*J;
    end;
    v=v+vi;
    dvdq=dvdq+dvidq;
end;

% Compute velocities of the vortices
vvort=zeros(2,N);
for ii=1:N;
    for jj=1:N;
        q=s(4+2*(ii-1)+1:4+2*(ii-1)+2)-s(4+2*(jj-1)+1:4+2*(jj-1)+2);
        q2=q'*q;
        vi=-kappa(jj)/2/pi*J*q;
        if q2>Q^2;
            vi=vi/q2;
        else
            vi=vi/Q^2;
        end;
        vvort(:,ii)=vvort(:,ii)+vi;
    end;
end;

% Define RHS (=ds)
ds=zeros(4+2*N,1);                          % Allocate memory
ds(1:2)=2/Eps*(p2-1)*s(3:4)*ksi+3*(pi^2)*v;   % Particle position
ds(3:4)=-3*(pi^2)*dvdq'*s(3:4);               % Particle momentum
ds(5:end)=0; %vvort(:)=0 - during the integration vortex positions are
             % frozen
```

Listing 2: This is the code to compute the equations of quasiparticles and vortices in Appendix B

```
clear all;

%This part of the code introduces parameters and variables necessary for
%calculations and organises thelinks with other subroutines of the code

%-------------------------------------------------------------------------
% Parameters
%-------------------------------------------------------------------------
t0=0; %initial moment for vortex motion
tmax=1000000;          % Maximum integration time for vortex dynamics
deltat=1000;        %timestep for vortex dynamics
tvector=t0:deltat:tmax;  % time vector
Nsteps=length(tvector); %number of steps for computation of vortex positions

box_size=500;  %size of quadratic computation box
bobox=[-box_size/2 -box_size/2 box_size/2 box_size/2]; %dimensions of
                                          %the box [xlb ylb xlt ylt];

tparticle=117; %maximum integration time for quasiparticles
               %(time parameter for ODE - solver odes15.)


Nt=1000;            % Number of points for plotting

%kappa=[1,1,1,1];    % Circulation, length of kappa must be equal to
                     %the number of vortices (+1 vortex, -1 antivortex).
%kappa=[1,1];

kappa=[1, 1,  1];

%kappa=1;
N=length(kappa); %number of vortices

ksi=934;  % Parameter describing the energy gap
Q=1;            % Inner radius of the vortices (size of vortex core)
filename='Data3vrts';    % vortex data is saved in this file
odefilename='reflcoef3vrts'; % reflection coefficents vs time
% Initial condition: s0=[qx; qy; px; py; qvort1; qvorty1; ...]

s0=[0; 0; 0; 0; -90;0; 77;50; -37;-80]; %3 vortices-2 vort,1 antivort
%s0=[-250;0;  1.0001;0;    -50;0;  0;50;  0;-50;  50;0];     % 4 vortices
%s0=[-250;-30;  1.0001;0;  0;-25;  0;25];     % 2 vortices
%s0=[-250;-0; 1.0001;0; 0;0];            % 1 vortex
qvort0=s0(5:end);   %Just positions of vortices

%-------------------------------------------------------------------------
%Processing and calculating vortex positions-----------------------------
%-------------------------------------------------------------------------
s=qvort0';

sol=zeros(Nsteps,(2*N)+1);
Nsol=length(sol);
sol(1,:)=[t0, qvort0'];
t=t0;

for ii=408:Nsteps-1 ;
    t=t+deltat;
    s=vortpos(deltat,s,kappa,Q,N); % subroutine containing eqs. of vortex
                                   % motions
    NS=length(s);

    s=checkbox(N,s,box_size); % subroutine setting the periodic conditions

    sol(ii+1,:)= [t,s']; % solution matrix

end
makeplots(sol, kappa, N, Nsteps, box_size); %plots vortex positions and
                                          %makes video - file.

%-------------------------------------------------------------------------
```

```
% Processing quasiparticles
%-------------------------------------------------------------------------
for ii=408:Nsteps-1  % Calculates quasiparticle dynamics at each timestep

 qv=sol(ii,2:end)'; %positions of vortices calculated above

 for jj=1:99 %calculates quasiparticle trajectories acroos y-axis

     qy=-250+jj*5;

     qp=[-250; qy; 1.0001; 0]; %  qp(1:2) - initial position of the
                               %quasiparticles, qp(3,4) - initial momentum
                               %of quasiparticles

     qs0=[qp;qv];

%tic                                                    % Start timer
options = odeset('RelTol',1e-8,'AbsTol',1e-8,'Stats','off');        % Set tolerances, increase AbsTol if
      code terminates.
qsol = ode15s(@odefun,[0 tparticle],qs0,options,kappa,ksi,Q);  % ODE solver, use ode45 or ode15s (stiff
     solver) if ode45 is slow
%toc                                                    % End timer

%-------------------------------------------------------------------------
% Post-processing
%-------------------------------------------------------------------------
%t=linspace(0,tmax,1995);
tq=linspace(0,tparticle,Nt);          % Define uniform grid for plotting
qs=deval(qsol,tq)'; % Evaluate solution on grid


r02=qs0(1)^2+qs0(2)^2; %initial distance of qua
p02=qs0(3)^2+qs0(4)^2;
Eps0=sqrt((p02-1)^2+1/ksi^2);
W(jj)=ksi*Eps0;

%-----------------------------------------------
%this block detects the reflection event---------
%-----------------------------------------------
if qs(end,1)<=-250
   refl=true;
   WRFL(jj)=W(jj);
else
   refl=false;
   WRFL(jj)=0;
end
 end
 %-----------------------------------------------
 totalflux=sum(W);
 Reflcflux=sum(WRFL);
 REFCOEF(ii)=Reflcflux/totalflux; %reflection coefficient vs time
 counter=ii
end
t=tvector(1:Nsteps-1);
save(filename,'sol');
save(odefilename,'t','REFCOEF'); % file contains Refl. coefs vs time.
odereflplot(odefilename); %plots refl. coefs vs time and its fourier
                          % transform power
```

Listing 3: This is the code to plot the graph of vortex positions and to create a movie of the trajectories of vortices

```
function makeplots(sol,kappa,N,Nsteps, box_size)

%plots of vortex positions and creates movie file.

for ii=1:1:Nsteps
    figurefile=[num2str(ii) '.png'];
    s=sol(ii,:);
    h=figure(ii);

   for jj=1:N
```

```
    x=s(1+2*jj-1); y=s(1+2*jj);
    if kappa(jj)==1
        plot(x,y,'r+');
        hold on
    else
        plot(x,y,'bo');
        hold on
    end
  end
  axis([-box_size/2 box_size/2 -box_size/2 box_size/2]);
   saveas(h,figurefile);
   print(h,'-dpng',figurefile);
   close(h)
end

writerObj = VideoWriter('3vortices.avi');
writerObj.FrameRate=4;
open(writerObj);
for K = 1 :5:Nsteps
  filename = sprintf('%d.png', K);
  thisimage = imread(filename);
  writeVideo(writerObj, thisimage);
  delete(filename)
end
close(writerObj);


delete('*.png');
```

Listing 4: This is the code to compute the Andreev reflection of quasiparticles

```
function odereflplot(filename)

RF=load(filename);

%plot 1: plots refl. coefs vs time
subplot(1,2,1)

plot(RF.t,RF.REFCOEF);

%-----------------------------------------------
% calculates power spectrum of ref. coef using function fft(X) - fast
% fourier transform
%-----------------------------------------------

Ntr=length(RF.REFCOEF); %length of the vector

FRS=abs(fft(RF.REFCOEF)); % Fourier transform of the vector

nu_min=1/(RF.t(end)-RF.t(1)); %minmum frequency
nus=1/(RF.t(2)-RF.t(1)); %frequency interval

NUFS=nus*(1:Ntr/2)/Ntr %frequency vector

%plots pover spectrum of FRS
Subplot(1,2,2)
plot(NUFS,FRS(1:Ntr/2));
```

Listing 5: This is the code to compute the position of vortices

```
function ds = vortpos(deltat,s,kappa,Q,N);

% calculates the vortex positions at time t.
% Number of vortices
s=s(:);

J=[[0,1];[-1,0]];


% Compute velocities of the vortices
vvort=zeros(2,N);
% deltat=10^(-3);     %delta t is time interval deltat=t-t0
```

```
for ii=1:N;
    for jj=1:N;
        q=s(2*(ii-1)+1:2*(ii-1)+2)-s(2*(jj-1)+1:2*(jj-1)+2); %initial coordinates of vortices
        q2=q'*q;
        vi=-kappa(jj)/2/pi*J*q;
        if q2>Q^2;
            vi=vi/q2;
        else
            vi=vi/Q^2;
        end
        vvort(:,ii)=vvort(:,ii)+vi;

    end

end
%problem: not sure if N and Nsteps iterations should be separated?

for ii=1:N;
    s(2*(ii-1)+1:2*(ii-1)+2)=s(2*(ii-1)+1:2*(ii-1)+2) + vvort(:,ii)*deltat; %new position of vortices
end


ds=s;
NS= length (ds);
```

B Appendix B

Equations below are used to run the codes in Appendix A

Equations of motion Dimensionless set of equations,

$$\frac{d}{dt}q_x = \frac{2}{\epsilon}(p^2-1)p_x + \frac{\pi}{\xi}v_x \tag{69}$$

$$\frac{d}{dt}q_y = \frac{2}{\epsilon}(p^2-1)p_y + \frac{\pi}{\xi}v_y \tag{70}$$

$$\frac{d}{dt}p_x = -\frac{\pi}{\xi}(p_x\frac{dv_x}{dq_x} + p_y\frac{dv_y}{dq_x}) \tag{71}$$

$$\frac{d}{dt}p_y = -\frac{\pi}{\xi}(p_x\frac{dv_x}{dq_y} + p_y\frac{dv_y}{dq_y}) \tag{72}$$

where

$$\epsilon = \sqrt{(p^2-1)^2+\xi^{-2}}, \quad p^2 = p_x^2 + p_y^2 \tag{73}$$

Equation 69-72 may be written in a more concise form

$$\frac{d}{dt}\mathbf{q} = \frac{2}{\epsilon}(|\mathbf{p}|^2-1)\mathbf{p} + \frac{\pi}{\xi}\mathbf{v} \tag{74}$$

$$\frac{d}{dt}\mathbf{p} = -\frac{\pi}{\xi}\left(\frac{d\mathbf{v}}{d\mathbf{q}}\right)^T \cdot \mathbf{p} \tag{75}$$

One vortex

For one vortex that is centered in the origin the velocity at the position of the particle is given by

$$\mathbf{v} = \begin{cases} \frac{-\kappa}{2\pi|\mathbf{q}|^2}\mathbf{J}\cdot\mathbf{q}, & |\mathbf{q}| > Q \\ \frac{-\kappa}{2\pi|Q^2}\mathbf{J}\cdot\mathbf{q}, & |\mathbf{q}| \leq Q \end{cases}$$

for $\mathbf{J}= \begin{bmatrix} 0 & 1 \\ -1 & 0 \end{bmatrix}$

where Q denotes the vortex radius and $\kappa = \pm$. Then the partial derivatives become

$$\frac{\mathbf{dv}}{\mathbf{dq}} = \begin{cases} \frac{\kappa}{2\pi|\mathbf{q}|^4}\begin{bmatrix} q_x q_y & q_y^2 \\ -q_x^2 & -q_x q_y \end{bmatrix} - \frac{\kappa}{2\pi|\mathbf{q}|^2}\mathbf{J}, & |\mathbf{q}| > Q \\ \frac{-\kappa}{2\pi Q^2}\mathbf{J}, & |\mathbf{q}| \leq Q \end{cases}$$

Many vortices The velocity $\mathbf{v}_i$ induced by each vortex V_i centered at $\mathbf{q}_i$, contributes to the velocity at the position $\mathbf{q}$,

$$\mathbf{v}(\mathbf{q}) = \sum_i \mathbf{v}_i(\mathbf{q})$$

and

$$\mathbf{v_i}(\mathbf{q}) = \begin{cases} \frac{-\kappa_i}{2\pi|\mathbf{q}-\mathbf{q}_i|^2}\mathbf{J}\cdot(\mathbf{q}-\mathbf{q}_i), & |\mathbf{q}-\mathbf{q}_i| > Q \\ \frac{-\kappa_i}{2\pi Q^2}\mathbf{J}\cdot(\mathbf{q}-\mathbf{q}_i), & |\mathbf{q}-\mathbf{q}_i| \leq Q \end{cases}$$

The partial derivatives are

$$\frac{d\mathbf{v}}{d\mathbf{q}} = \sum_i \frac{d\mathbf{v_i}}{d\mathbf{q}}$$

with

$$\frac{d\mathbf{v}_i}{d\mathbf{q}} = \begin{cases} \frac{\kappa_i}{\pi|\mathbf{q}-\mathbf{q}_i|^4}\begin{bmatrix} (q_x-q_{xi})(q_y-q_{yi}) & (q_y-q_{yi})^2 \\ -(q_x-q_{xi})^2 & -(q_x-q_{xi})(q_y-q_{yi}) \end{bmatrix} - \frac{-\kappa_i}{2\pi\mathbf{q}-\mathbf{q}_i|^2}\mathbf{J} & |\mathbf{q}-\mathbf{q}_i| > Q \\ \frac{-\kappa_i}{2\pi|Q^2}\mathbf{J}, & |\mathbf{q}-\mathbf{q}_i| \leq Q \end{cases}$$

Each vortex moves in the velocity field that is generated by the other vortices :

$$\frac{d\mathbf{q}_i}{dt} = \sum_{j\neq i} \mathbf{v}_j(\mathbf{q}_i)$$